Maneuvering Control of Planar Snake Robots Using Virtual Holonomic Constraints

Alireza Mohammadi, Ehsan Rezapour, Manfredi Maggiore, *Member, IEEE,* and Kristin Y. Pettersen, *Senior Member, IEEE*

***Abstract*—This paper investigates the problem of maneuvering control for planar snake robots. The control objective is to make the center of mass of the snake robot converge to a desired path and traverse the path with a desired velocity. The proposed feedback control strategy enforces virtual constraints encoding a lateral undulatory gait, parametrized by states of dynamic compensators used to regulate the orientation and forward speed of the snake robot.**

***Index Terms*—Virtual holonomic constraints, biologically inspired robot, path following, snake robot, hierarchical control, reduction theorems, stability of closed sets.**

I. Introduction

Inspired by biological snakes, snake robots are underactuated vehicle-manipulator systems with many degrees-of-freedom that can effectively be used for operations in challenging environments. The large number of degrees-of-freedom enables snake robots to operate on irregular and cluttered surfaces, to climb stairs, and to even climb on poles. Snake robots pose significant motion control challenges arising from the fact that such robots typically have at least three degrees of underactuation.

One of the basic gait patterns through which biological snakes achieve forward motion is called lateral undulation [1]. During lateral undulation, the snake undergoes periodic shape changes that resemble a wave traveling backward along its body, from head to tail. As a result of this motion, the snake body traces out a periodic curve on the plane, which Hirose [1] mathematically represented as a *serpenoid*. Thinking of a snake robot as a discrete approximation of a biological snake, researchers (see, e.g.,[1], [2], [3]) have observed that the serpenoid curve can be well-approximated by imposing the sinusoidal reference signal for the i^{th} joint angle

$$\phi_{\text{ref},i}(t) = \alpha \sin(\omega t + (i-1)\delta) + \phi_0, \tag{1}$$

where α denotes the amplitude of the sinusoid, ω denotes the frequency of the joint oscillations, δ denotes the phase shift between two consecutive joints, and ϕ_0 is a joint offset used to control the direction of locomotion.

Snake robots can be broadly classified as nonholonomic or holonomic. Nonholonomic snake robots have passive wheels on each link that are subject to nonholonomic velocity constraints. The world's first snake robot, developed in 1972 ([1]) belongs to this class, and to date the bulk of research on snake robotics focuses on robots using passive wheels. The typical approach for locomotion control of nonholonomic snake robots is to use the sideslip constraints to define the control input directly in terms of the desired propulsion of the robot. This technique is employed in [4], [5], [6] for computed torque control of the position and heading of snake robots. In [7], a path following controller is proposed for the case where some, but not all, of the snake robot links are subject to sideslip constraints. These constrained links can be lifted off the ground, giving DOFs that can be utilized to follow a trajectory while simultaneously maintaining a high manipulability. Similar approaches are considered in [8], where strategies for sinus-lifting during the lateral undulatory motion are proposed. In [9], a path following controller is proposed, and a Lyapunov stability analysis is presented.

Holonomic snake robots do not have passive wheels, and exploit friction for locomotion. The motion of holonomic snake robots mimics closely the motion of their biological counterparts [10]. This is due to the possibility of sideways motion, which enables the robot to perform various types of gait patterns used by biological snakes. However, unlike the snake robots with sideslip constraints, locomotion control of this class of snake robots has been considered in only a few previous works. One of the reasons might be that holonomic snake robots are harder to control. Indeed, for nonholonomic snake robots only the kinematics has to be considered when describing the snake robot motion because one may use velocity as the control input to the joints of the robot. On the other hand, in holonomic snake robots, both the dynamics and kinematics have to be considered in analysis and control design in that the propulsion mechanism is the complex interplay between joint friction forces and center of mass forces. The resulting dynamical model is underactuated, something which poses additional challenges for control design. In [11], path following control of swimming snake robots is achieved by moving the joints according to a predetermined gait pattern while introducing an angular offset in each joint to reorient the robot towards a desired path. Methods based on numerical optimal control are considered in [12] for determining optimal gaits during positional control of snake robots. In [13], a control strategy is proposed for sinus-lifting during lateral undulation by solving a quadratic

A. Mohammadi and M. Maggiore were supported by the Natural Sciences and Engineering Research Council (NSERC) of Canada. A. Mohammadi was also supported in part by the Ontario Graduate Scholarship (OGS). E. Rezapour and K. Y. Pettersen were partly supported by the Research Council of Norway through the Centres of Excellence funding scheme, project No. 223254 AMOS, and project No. 205622.

A. Mohammadi and M. Maggiore are with the Department of Electrical and Computer Engineering, University of Toronto, 10 King's College Road, Toronto, ON M5S 3G4, Canada. E-mail: alireza.mohammadi@mail.utoronto.ca, maggiore@control.utoronto.ca

E. Rezapour is with Norsk Titanium AS in Honefoss, Norway. E-mail: ehsan.rezapour@itk.ntnu.no

K. Y. Pettersen is with the Department of Engineering Cybernetics, Norwegian University of Science and Technology, NO-7491 Trondheim, Norway. E-mail: Kristin.Y.Pettersen@itk.ntnu.no

Published in *IEEE Transactions on Control Systems Technology,* vol. 24, no. 3, pp. 884–899, 2016

optimization problem. In [14], two physical parameters, constraint forces and energy efficiency are introduced as cost functions to optimize, and switching strategies are proposed for generating optimal motion patterns of a snake like robot. In [15], a framework has been put forward which allows a planner to generate paths in a low dimensional work space and select among gaits, pre-planned motions in the robot's shape space. In [16], modal decomposition has been used to modify a snake robots sidewinding gait to orient the head during locomotion.

In [17], numerical simulations are used to study the properties of lateral undulation that are related to the optimality of motion of the robot. In [18], controllability and stabilizability of planar snake robot locomotion is considered, and stability results for a path following controller based on numerical investigations using Poincaré map are presented. In [19], cascaded systems theory is employed to achieve straight line path following control of a snake robot described by the simplified model presented in [10]. In this simplified model of the snake robot, the motion of the links is approximated as translational motion instead of rotational motion, which is valid for small joint angles.

In [20], a dynamic feedback controller is proposed which controls the orientation of the robot to an angle that is defined by a path following guidance law which makes the robot follow a straight line. In [21], the theoretical approaches presented in [20] are validated through experimental results. In [22], using the method of virtual holonomic constraints, a direction following controller is proposed which regulates the orientation and the forward velocity of the robot to constant references. A similar approach is used in [23], where the design is based on the simplified dynamic model presented in [10]. In [24], by utilizing the direction following controller of [23] and the path following controller of [19], a maneuvering controller is proposed based on the simplified model for snake robots which makes the robot converge to and follow a straight line path with a desired forward velocity. However, neither of the above works have reported results for path following control along general curved paths based on complete kinematic and dynamic models of snake robots. A complete review on modelling and control of snake robots can be found in [25]. The typical control approach in the snake locomotion literature relies on the asymptotic tracking of suitably designed reference signals, such as (1).

Contributions of this paper. In this paper we investigate the following maneuvering problem: make the center of mass of a holonomic snake robot converge to a desired path and traverse the path with some desired velocity while guaranteeing boundedness of the system states. Our proposed controller has a three-stage hierarchical structure. A virtual constraint encoding a lateral undulatory gait is stabilized at the lowest level of the hierarchy. In the next level of the hierarchy, the velocity of the center of mass of the snake robot is regulated to some desired reference vector. The desired reference vector is determined at the top level of the hierarchy using a path following controller designed for a kinematic point-mass system. The block diagram of the proposed controller is depicted in Figure 2. Using the proposed hierarchical structure and based on the complete model of snake robot we solve the path following control problem along any desired path which can be considered as an important step forward in locomotion control of snake robots and similar multi-link robotic structures.

Another contribution of the paper is that we propose an approach that removes timed signals entirely from the control loop, and replaces them with state-dependent constraints. Specifically, we replace the time-dependent term ωt in the lateral undulatory gait (1) with the state λ of a compensator, modify the way in which the offset ϕ_0 affects the gait, and view this offset as the state of a second compensator. The result is a state-dependent undulatory gait which can be considered as a dynamic virtual constraint. Virtual constraints have been successfully used in the robot locomotion literature [26], [27] and have been investigated in the general context of Euler-Lagrange control systems [28], [29]. By eliminating exogenous reference signals, virtual constraints enhance the robustness of the feedback loop and add flexibility to the control design.

Comparison with existing literature. Previous research on position and path following control of holonomic snake robots is very limited but is considered in e.g. [12], [11], [18], and [19]. The paper [18] was the first work to present a stability analysis of the locomotion along a straight path. Being based on a numerical Poincaré test, the analysis in [18] is only valid for a specific set of controller parameters. In [19], path following control of snake robots along straight paths is considered. Using cascaded systems theory, it is proved that the proposed path following controller $\mathcal{K}$-exponentially stabilizes a snake robot to any desired straight path. A drawback of [19] is that the stability analysis is valid for a simplified model which is only valid for small joint angles. Another drawback of [18] and [19] is that they are only valid for straight lines and not all curved paths. To the best of our knowledge, to date there is no proof of convergence of a path following controller for the complete nonlinear model of a holonomic snake robot. Moreover, the control schemes in the existing literature do not control speed.

This paper presents the first control methodology applicable to the complete nonlinear model of a holonomic snake robot, with guaranteed stability properties. The methodology we propose is applicable to general paths, and in addition to make the snake follow the path, it regulates the speed of the center of mass. In particular, we establish a clear link between frequency of oscillations ($\dot{\lambda}$) and speed.

Organization of the paper. In Section II, we present mathematical preliminaries dealing with the reduction theorems for stability of closed sets which will be used later in the paper. In Section III, we present the kinematic and dynamic model of the snake robot. In Section IV, we state the control design objectives. In Section V, we consider the shape control for the robot. In Sections VI-A and VI-B, we develop control strategies for the head angle and the speed of the robot, respectively. In Section VII, we develop a path following control strategy. In Section VIII, we present the main result of the paper. Finally, Section IX presents simulation results which illustrate the performance of the proposed control strategy.

Notation. Given a vector $x \in \Re^N$, we denote by $\|x\|$ the

Euclidean norm of x. Given a matrix $X \in \Re^{m\times n}$, we denote by $\|X\|_p$ the induced p-norm of X. Given a set $\Gamma \subset \Re^N$ and a point $x \in \Re^N$, we define the point-to-set distance of x to Γ to be $\|x\|_\Gamma := \inf\{\|x-y\| : y \in \Gamma\}$. Let $a \in \Re$, then a modulo 2π is denoted by $[a]_{2\pi}$. The set $[\Re]_{2\pi} = \{[a]_{2\pi} : a \in \Re\}$ can be given a manifold structure which makes it diffeomorphic to the unit circle S^1. Finally, we denote the complex plane by $\mathbb{C}$. Following the notation in [10], we make use of the following matrices and vectors

$$A = \begin{bmatrix} 1 & 1 & 0 & \dots & 0 \\ 0 & 1 & 1 & \dots & 0 \\ & \dots & & & \\ 0 & 0 & \dots & 1 & 1 \end{bmatrix} \in \Re^{(N-1)\times N}$$

$$D = \begin{bmatrix} 1 & -1 & \dots & 0 & 0 \\ 0 & 1 & -1 & \dots & 0 \\ & \dots & & & \\ 0 & 0 & \dots & 1 & -1 \end{bmatrix} \in \Re^{(N-1)\times N}$$

$$e = [1,\dots,1]^T \in \Re^N$$

$$E = \begin{bmatrix} e & 0_{N\times 1} \\ 0_{N\times 1} & e \end{bmatrix} \in \Re^{2N\times 2}$$

$$\bar{e} = [1,\dots,1]^T \in \Re^{N-1},\ \boldsymbol{\theta} = [\theta_1,\dots,\theta_N]^T \in \Re^N$$

$$\sin\boldsymbol{\theta} = [\sin\theta_1,\dots,\sin\theta_N]^T \in \Re^N$$

$$\cos\boldsymbol{\theta} = [\cos\theta_1,\dots,\cos\theta_N]^T \in \Re^N$$

$$S_{\boldsymbol{\theta}} = \mathrm{diag}(\sin\boldsymbol{\theta}) \in \Re^{N\times N}$$

$$C_{\boldsymbol{\theta}} = \mathrm{diag}(\cos\boldsymbol{\theta}) \in \Re^{N\times N}$$

$$\dot{\boldsymbol{\theta}}^2 = \left[\dot\theta_1^2,\dots,\dot\theta_N^2\right]^T \in \Re^N$$

$$b = [0,\dots,0,1]^T \in \Re^{N-1}$$

$$H = \begin{bmatrix} 1 & 1 & \dots & 1 \\ 0 & 1 & \dots & 1 \\ & \dots & & \\ 0 & 0 & \dots & 1 \\ 0 & 0 & \dots & 0 \end{bmatrix} \in \Re^{N\times(N-1)}$$

$$I_N = \begin{bmatrix} 1 & & & \\ & 1 & & \\ & & \dots & \\ & & & 1 \end{bmatrix} \in \Re^{N\times N}$$

$$V = A^T(DD^T)^{-1}A$$

$$K = A^T(DD^T)^{-1}D$$

$$SC_{\boldsymbol{\theta}} = \begin{bmatrix} K^T S_{\boldsymbol{\theta}} \\ -K^T C_{\boldsymbol{\theta}} \end{bmatrix}$$

II. Preliminaries

As discussed in the introduction, the control design approach taken in this paper is hierarchical in that the design is broken down in three stages corresponding to three prioritized control specifications. As we show shortly, each specification corresponds to the stabilization of a suitable closed subset of the state space of the snake robot. In this section we present the theoretical tool that enables the hierarchical decomposition of the control task: a so-called reduction theorem for stability of nested closed sets, [30], [31]. In this subsection, we present for completeness the version of the reduction theorem that we use in the paper. This theorem may be used in applications in which the designer must simultaneously meet control specifications that can be formulated hierarchically. Consider the dynamical system

$$\Sigma: \quad \dot{x} = f(x,u) \tag{2}$$

with the state space $\mathcal{X} \subset \mathbb{R}^n$, where f is locally Lipschitz on $\mathcal{X}$, with the solution $\phi(t,x_0)$ at time t and initial condition $x(0) = x_0$, and $u(x)$ is a locally Lipschitz feedback which makes the sets $\Gamma_1 \subset \Gamma_2$ positively invariant for the closed-loop system. This invariance property implies that for all $x_0 \in \Gamma_i$, $i = 1,2$, and for all $t \geq 0$, $\phi(t,x_0) \in \Gamma_i$. Furthermore, we say that the set Γ_1 is (globally) asymptotically stable *relative* to Γ_2 for Σ, provided that whenever $x_0 \in \Gamma_2$ then Γ_1 is (globally) asymptotically stable. Specifically, we have the following definition.

Definition 2.1. Let Γ_1 and Γ_2, $\Gamma_1 \subset \Gamma_2 \subset \mathcal{X}$, be closed positively invariant sets. We say that Γ_1 is stable relative to Γ_2 for Σ if, for any $\varepsilon > 0$, there exists a neighbourhood $\mathcal{N}(\Gamma_1)$ such that $\phi(\mathbb{R}_{>0}, \mathcal{N}(\Gamma_1) \cap \Gamma_2) \subset \mathcal{B}_\varepsilon(\Gamma_1)$ where $\phi(\mathbb{R}_{>0}, \mathcal{N}(\Gamma_1) \cap \Gamma_2)$ denotes the set $\{\phi(t,x_0) : t \in \mathbb{R}_{>0},\ x_0 \in \mathcal{N}(\Gamma_1) \cap \Gamma_2\}$. △

In the above definition, $\mathcal{B}_\varepsilon(\Gamma_1)$ denotes the ε-ball given by the set $\mathcal{B}_\varepsilon(\Gamma_1) = \{x \in \mathcal{X} :\ \|x\|_{\Gamma_1} < \varepsilon\}$.

Now suppose that $\Gamma_1 \subset \Gamma_2 \subset \ldots \subset \Gamma_l$ is a nested sequence of closed subsets of $\mathcal{X}$ which represent hierarchical control specifications. Specifically, each set Γ_i is associated with a control specification i. The property that $\Gamma_i \subset \Gamma_{i+1}$ implies that specification i is met only if specification $i+1$ is met, so that specification $i+1$ has higher priority than specification i. Therefore, the list of nested subsets Γ_i is associated with a hierarchy of control specifications.

We state Part (a) of Proposition 14 in [31], and we will use this to carry out the control design and to prove the main result of our paper.

Proposition 2.2 ([31])**.** *Consider system (1), and assume that there exists a locally Lipschitz feedback $\overline{u}(x)$ making the sets $\Gamma_1 \subset \Gamma_2 \subset \ldots \subset \Gamma_l$, positively invariant for the closed-loop system. Let $\Gamma_{l+1} := \mathcal{X}$. If, for $i = 1,\dots,l$, Γ_i is asymptotically stable relative to Γ_{i+1} for the closed-loop system, and Γ_1 is compact, then Γ_1 is asymptotically stable for the closed-loop system $\dot{x} = f(x,\overline{u}(x))$.*

Before concluding this section, we define an operator which will be useful in proving an important relationship later in the paper.

Definition 2.3. The complexification operator is defined to be the map $\mathfrak{C} : \Re^2 \to \mathbb{C}$, $[x,y]^T \mapsto x + jy$, where j is the unit imaginary number. △

According to the above definition, it can be easily seen that the operator $\mathfrak{C}$ is a linear invertible map, i.e., an isomorphism from the real plane to the complex plane. We have the following lemma whose proof is omitted due to simplicity.

Lemma 2.4. *Given the counter-clockwise rotation matrix $R_\theta \in \Re^{2\times 2}$ through an angle θ and a vector $[x, y]^T \in \Re^2$, we have $\mathfrak{C}(R_\theta [x, y]^T) = \exp(j\theta)(x + jy)$, where $\exp(j\theta) = \cos(\theta) + j \sin(\theta)$.*

III. Model of the Snake Robot

In this section, we review the kinematic and dynamic model of a snake robot presented in [10]. We consider a snake robot with N rigid links each of length $2l$. Each link is assumed to have uniformly distributed mass m and moment of inertia J. We denote the vector of absolute link angles by $\boldsymbol{\theta} = [\theta_1, \ldots, \theta_N]^T \in \Re^N$, and the center of mass of the robot in inertial coordinates by $p = [p_x, p_y]^T \in \Re^2$. Also, we denote the vector of joint angles by $\phi = [\phi_1, \ldots, \phi_{N-1}]^T$, where $\phi_i = \theta_i - \theta_{i+1}$ denote the i^{th} joint angle. Figure 1 illustrates the kinematic parameters of the snake robot. Table I summarizes the parameters of the snake robot used in our simulations. Following [10], the dynamic equations of the snake robot can be written as follows

$$M_{\boldsymbol{\theta}} \ddot{\boldsymbol{\theta}} + W_{\boldsymbol{\theta}} \dot{\boldsymbol{\theta}}^2 - lSC_{\boldsymbol{\theta}}^T f_R(\boldsymbol{\theta}, \dot{\boldsymbol{\theta}}, \dot{p}) = D^T u, \tag{3a}$$
$$Nm\ddot{p} = E^T f_R(\boldsymbol{\theta}, \dot{\boldsymbol{\theta}}, \dot{p}), \tag{3b}$$

where $u \in \Re^{N-1}$ is the vector of actuator torques, $f_R(\cdot) \in \Re^2$ is the vector of ground friction forces, and the remaining quantities are defined as follows:

$$M_{\boldsymbol{\theta}} = JI_N + ml^2 S_{\boldsymbol{\theta}} V S_{\boldsymbol{\theta}} + ml^2 C_{\boldsymbol{\theta}} V C_{\boldsymbol{\theta}}, \tag{4a}$$
$$W_{\boldsymbol{\theta}} = ml^2 S_{\boldsymbol{\theta}} V C_{\boldsymbol{\theta}} - ml^2 C_{\boldsymbol{\theta}} V S_{\boldsymbol{\theta}}. \tag{4b}$$

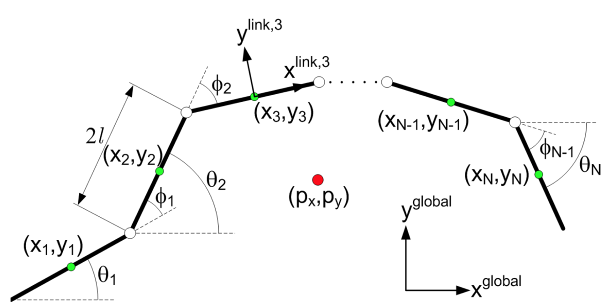

Fig. 1. Kinematic parameters of the snake robot.

The mechanical system (3a)-(3b) has $N + 2$ configuration variables and $N - 1$ controls. It therefore has three degrees of underactuation. The actuator torques have no direct effect on the center of mass dynamics (3b). The only coupling between the joint dynamics (3a) and center of mass dynamics (3b) occurs through the ground friction force f_R. This coupling is the essential mechanism underlying snake locomotion, and it is what makes the motion control problem challenging.

TABLE I
THE PARAMETERS OF THE SNAKE ROBOT

Symbol	Description	Numerical values in simulations
N	Number of links.	10
$2l$	Length of a link.	0.14 m
m	Mass of a link.	1 kg
$\boldsymbol{\theta} \in \Re^N$	Vector of absolute link angles.	–
$\boldsymbol{\phi} \in \Re^{N-1}$	Vector of joint angles.	–
$p = [p_x, p_y] \in \Re^2$	CM position of the robot.	–
c_t	Tangential viscous friction coefficient.	0.5
c_n	Normal viscous friction coefficient.	3

For simplicity, we assume that the friction forces acting on the robot are viscous. A snake robot which is subject to viscous friction qualitatively (although not quantitatively) behaves similarly to a snake robot which is subject to Coulomb friction force [10]. We have:

$$\begin{aligned} f_R(\boldsymbol{\theta}, \dot{\boldsymbol{\theta}}, \dot{p}) &= \begin{bmatrix} f_{R,x} \\ f_{R,y} \end{bmatrix} = Q_{\boldsymbol{\theta}} \begin{bmatrix} \dot{X} \\ \dot{Y} \end{bmatrix} \\ &= Q_{\boldsymbol{\theta}} \begin{bmatrix} lK^T S_{\boldsymbol{\theta}} \dot{\boldsymbol{\theta}} + e\dot{p}_x \\ -lK^T C_{\boldsymbol{\theta}} \dot{\boldsymbol{\theta}} + e\dot{p}_y \end{bmatrix} = lQ_{\boldsymbol{\theta}} SC_{\boldsymbol{\theta}} \dot{\boldsymbol{\theta}} + Q_{\boldsymbol{\theta}} E\dot{p} \end{aligned} \tag{5}$$

where $X = [x_1, \ldots, x_N] \in \Re^N$, $Y = [y_1, \ldots, y_N] \in \Re^N$ are the vectors of inertial coordinates of the centers of mass of the links of the robot. The matrix $Q_{\boldsymbol{\theta}}$ maps the inertial frame velocities of the centers of mass of the links to the inertial frame viscous friction forces acting on the links, and it is given by

$$Q_{\boldsymbol{\theta}} = -\begin{bmatrix} c_t(C_{\boldsymbol{\theta}})^2 + c_n(S_{\boldsymbol{\theta}})^2 & (c_t - c_n)S_{\boldsymbol{\theta}} C_{\boldsymbol{\theta}} \\ (c_t - c_n)S_{\boldsymbol{\theta}} C_{\boldsymbol{\theta}} & c_t(S_{\boldsymbol{\theta}})^2 + c_n(C_{\boldsymbol{\theta}})^2 \end{bmatrix}, \tag{6}$$

where c_t and c_n denote the tangential and normal viscous friction coefficients of the links, respectively. In this paper, inspired by biological snakes, we assume that $c_n > c_t$. This assumption implies that each link is subjected to an anisotropic viscous ground friction force, which means that the ground friction normal to the link is larger than the ground friction parallel to the link. It is shown in [10] that propulsion of a snake robot under viscous friction conditions requires the friction to be anisotropic. In practice, one may achieve anisotropic friction on the links by equipping the underside of each link of the robot with edges, or grooves, that run parallel to each link.

Remark 3.1. One can use the custom testbed constructed in [32] to specify the numerical value of c_t and c_n. This testbed utilizes a pulley, a motor, and a load cell to measure the required forces for moving the joint module along the locomotion substrate at different velocities. As it will be shown in Section IX, our controller shows some degree of robustness with respect to uncertainties in c_t and c_n. △

Finally, letting $u_{\theta_N} = [\cos\theta_N, \sin\theta_N]^T$ and $v_{\theta_N} = [-\sin\theta_N, \cos\theta_N]^T$, we define

$$v_t = u_{\theta_N}^T \dot{p}, \tag{7a}$$
$$v_n = v_{\theta_N}^T \dot{p}. \tag{7b}$$

The scalars v_t and v_n defined above are the components of the inertial velocity of the center of mass parallel and perpendicular to the angle of the head, respectively. According to (7a) and (7b), the map $[v_t, v_n]^T \mapsto \dot{p}$ is a diffeomorphism given by

$$\dot{p} = R_{\theta_N} \begin{bmatrix} v_t \\ v_n \end{bmatrix}. \tag{8}$$

IV. Control Specifications

In this section we present the blueprint of our control design. Figure 2 depicts the diagram of the proposed controller. We begin by stating the control specifications.

Velocity Control Problem (VCP): Given a desired velocity vector $\mu(p)$ with polar representation

$$\mu(p) = v_{\text{ref}}(p) \begin{bmatrix} \cos(\theta_{\text{ref}}(p)) \\ \sin(\theta_{\text{ref}}(p)) \end{bmatrix}, \tag{9}$$

design a smooth feedback controller achieving the following specifications:

(i) Practical stabilization[1] of the head angle θ_N to $\theta_{\text{ref}}(p)$.
(ii) Practical stabilization of the tangential velocity $v_t = u_{\theta_N}^T \dot{p}$ to $v_{\text{ref}}(p)$.
(iii) Uniform ultimate boundedness of the normal velocity $v_n = v_{\theta_N}^T \dot{p}$ with a small ultimate bound, and ultimate boundedness of the solutions of the joint dynamics and all controller states.

The above problem formulation relies on the observation that if $\theta_N = \theta_{\text{ref}}(p)$, then making $\dot{p} \to \mu(p)$ is equivalent to making $(v_t, v_n) \to (v_{\text{ref}}(p), 0)$.

Path Following Problem (PFP): Given a desired continuously differentiable curve $\gamma \subset \Re^2$ with implicit representation $\{p \in \Re^2 : h(p) = 0\}$ with $dh_p \neq 0$ on γ, design a smooth feedback controller achieving the following specifications:

(i) Path stabilization: make $p(t) \to \gamma$.
(ii) Velocity control: make $\|\dot{p}\| = v$ on γ, where v is the desired speed on the path γ.

The first control specification, i.e., the VCP, will be used to achieve the second control specification, i.e., the PFP.

Solution Methodology:

In order to solve VCP and PFP, we create a hierarchy of three control specifications, resulting in a three-stage control design.

Stage 1: Body Shape Control. We use the controls u in (3a) to stabilize a virtual constraint encoding a lateral undulatory gait similar to (1), in which ωt is replaced by a state λ, and ϕ_0 affects only the head angle θ_N. The evolution of λ, ϕ_0 is governed by two compensators, $\ddot{\phi}_0 = u_{\phi_0}$ and $\ddot{\lambda} = u_\lambda$.

Stage 2: Velocity Control. Given a desired velocity function $\mu(p)$ as in (9), this stage unfolds in two substages:

A. Head Angle Control. Inspired by the biological observation that snakes keep their head pointed towards a target while their body undulates behind the head, we design u_{ϕ_0} to practically stabilize $\theta_N \to \theta_{\text{ref}}(p)$ while guaranteeing that $(\phi_0, \dot{\phi}_0)$ is uniformly ultimately bounded.

B. Speed Control. We design u_λ to practically stabilize $v_t \to v_{\text{ref}}(p)$ while guaranteeing that v_n settles into a small neighborhood of the origin and $\dot{\lambda}$ is uniformly ultimately bounded.

Stage 3: Path Following Control. Design the velocity function $\mu(p)$ in (9) such that when $\|\dot{p} - \mu(p)\|$ is sufficiently small, PFP is solved.

Remark 4.1. The above design methodology is based on the following intuition. The first priority in the control of the robot is to induce forward motion on the snake robot which is achieved through body shape control according to lateral undulation. The second priority is the orientation control which can orient the robot towards a target in the plane, together with the velocity control that makes the robot move towards this target. Finally, we would like to have position control which makes the robot move along the desired path. If we remove the intermediate velocity control, the robot won't track the desired path. △

As discussed in the introduction, snake robots move forwards by tracing out a periodic curve. Because of this oscillatory motion, the head angle and velocity tangential and normal to the snake motion will not be constant, but rather oscillate around their steady state values. This is the reason why practical stability is sought, as opposed to asymptotic stability of constant values which is not a feasible control objective for the snake robot locomotion.

V. Body Shape Control

In this section, we use the control inputs u in (3a) to stabilize a lateral undulatory gait for the shape variables of the robot. Inspired by the lateral undulatory gait in (1), we stabilize the relations:

$$\theta_i - \theta_{i+1} = \alpha \sin(\lambda + (i-1)\delta),\ i = 1, \ldots, N-2, \tag{10a}$$
$$\theta_{N-1} - \theta_N = \alpha \sin(\lambda + (N-2)\delta) + \phi_0, \tag{10b}$$

where (α, δ) are positive constants referred to as gait parameters and $(\lambda, \phi_0) \in S^1 \times \Re$ are the states of two compensators

$$\ddot{\lambda} = u_\lambda,\ \ddot{\phi}_0 = u_{\phi_0}, \tag{11}$$

to be designed later. The relations (10a)–(10b) are referred to as virtual holonomic constraints (VHC) [28], [29], and they have the property that they can be made invariant through feedback control. These VHCs are parametrized by the states of the dynamic compensators in (11) which will be used to control the orientation and position of the robot in the plane.

[1] Practical stabilization of a variable means that by a suitable choice of controller parameters the variable is made to converge to an arbitrarily small neighborhood of its desired value.

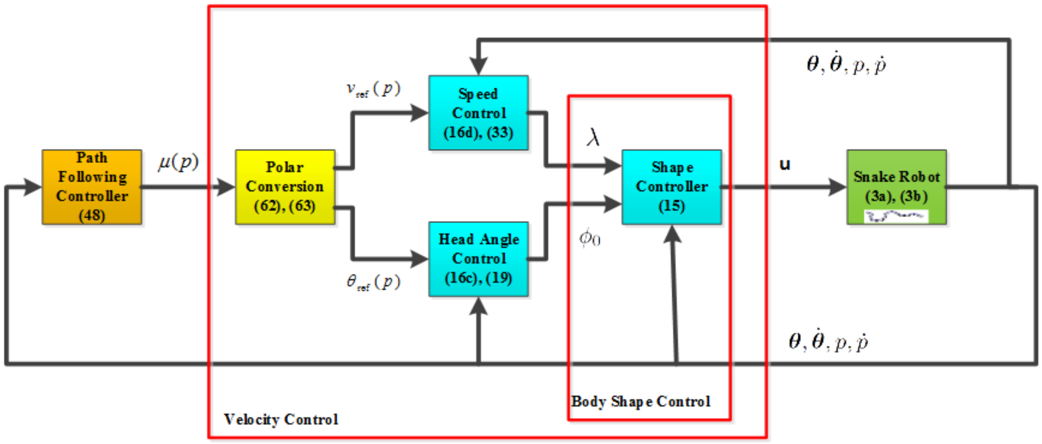

Fig. 2. The proposed path following controller is comprised of three stages, corresponding to the three loops of the block diagram. Stage 1, body shape control, stabilizes an undulatory gait pattern. This stage corresponds to the inner-most control loop, and it has the highest priority. The second stage, velocity control, regulates the velocity vector of the snake's center of mass to a reference. The third stage, path following control, produces a velocity vector reference for Stage 2, given by $\mu(p)$, making the snake robot move towards and along the desired path. This stage corresponds to the outer-most control loop, and it has lowest priority.

Let $\Phi_i(\lambda) = \alpha \sin(\lambda + (i-1)\delta), i = 1, \ldots, N-1$ and $\Phi(\lambda) = [\Phi_1(\lambda), \ldots, \Phi_{N-1}(\lambda)]^T \in \Re^{N-1}$. Since $\boldsymbol{\theta} = HD\boldsymbol{\theta} + e\theta_N$, the relations in (10a)-(10b) can be expressed in vector form as follows:

$$\boldsymbol{\theta} = e\theta_N + H\Phi(\lambda) + Hb\phi_0. \tag{12}$$

The above can also be written as $\mathfrak{h}(\lambda, \phi_0, \boldsymbol{\theta}) = 0$, where

$$\mathfrak{h}(\lambda, \phi_0, \boldsymbol{\theta}) = D\boldsymbol{\theta} - \Phi(\lambda) - b\phi_0. \tag{13}$$

If we view $\mathfrak{h}(\lambda, \phi_0, \boldsymbol{\theta})$ as an output function for system (3) augmented with compensators (11), then this output yields a vector relative degree $\{2, \ldots, 2\}$ everywhere because $\mathrm{rank}(DM_{\boldsymbol{\theta}}^{-1}D^T) = N-1$. Consequently, the zero dynamics manifold associated with output (13) is the set

$$\begin{aligned}\Gamma_3 = \{(\boldsymbol{\theta}, \dot{\boldsymbol{\theta}}, p, \dot{p}, \lambda, \dot{\lambda}, \phi_0, \dot{\phi}_0) \in \Re^{2N+8} : D\boldsymbol{\theta} = \Phi(\lambda) + b\phi_0,\\ D\dot{\boldsymbol{\theta}} = \Phi^{'}(\lambda)\dot{\lambda} + b\dot{\phi}_0\}.\end{aligned} \tag{14}$$

We refer to Γ_3 as the constraint manifold associated with the VHC (10) (the virtual constraint manifold). Stabilizing the VHC (10) corresponds to stabilizing Γ_3. To this end, we use the input-output linearizing control law

$$\begin{aligned}u = {} & (DM_{\boldsymbol{\theta}}^{-1}D^T)^{-1}\{DM_{\boldsymbol{\theta}}^{-1}W_{\boldsymbol{\theta}}\dot{\boldsymbol{\theta}}^2\\ & -lDM_{\boldsymbol{\theta}}^{-1}SC_{\boldsymbol{\theta}}^T f_R + \Phi^{''}(\lambda)\dot{\lambda}^2 + \Phi^{'}(\lambda)u_\lambda\\ & +bu_{\phi_0} - K_P[D\boldsymbol{\theta} - \Phi(\lambda) - b\phi_0]\\ & -K_D[D\dot{\boldsymbol{\theta}} - \Phi^{'}(\lambda)\dot{\lambda} - b\dot{\phi}_0]\},\end{aligned} \tag{15}$$

where K_D, K_P are positive definite diagonal matrices containing the joint controller gains.

Remark 5.1. Under the assumption $c_n > c_t$, it can be shown that $\frac{c_t}{\sqrt{N}} \leq \|Q_{\boldsymbol{\theta}}\|_2 \leq 1.2071c_n - 0.2071c_t$ because $\frac{1}{\sqrt{N}}\|Q_{\boldsymbol{\theta}}\|_1 \leq \|Q_{\boldsymbol{\theta}}\|_2 \leq \sqrt{\|Q_{\boldsymbol{\theta}}\|_1\|Q_{\boldsymbol{\theta}}\|_\infty}$ (see [33]). On the other hand, $\|Q_{\boldsymbol{\theta}}\|_1 = \|Q_{\boldsymbol{\theta}}\|_\infty = \max_{1\leq i\leq N}\{c_t\cos(\theta_i)^2 + c_n\sin(\theta_i)^2 + \frac{c_n - c_t}{2}|\sin(2\theta_i)|\} = \max_{1\leq i\leq N}\{c_t + \frac{c_n-c_t}{2}(2\sin(\theta_i)^2 + |\sin(2\theta_i)|)\}$. Therefore, the ground friction force magnitude $\|f_R(.)\|$ increases with increasing friction coefficients c_n and c_t according to (5). This shows the dependence of motor control torques given by (15) on the friction coefficients c_n and c_t. $\triangle$

After asymptotically stabilizing Γ_3, we are left with two control inputs, (u_λ, u_{ϕ_0}) to solve the direction following problem. As described in Section IV we will use the dynamic compensators to regulate the head angle and the velocity of the robot to desired values. To this end, we first derive the reduced dynamics of the robot, i.e., we reduce the system to the invariant manifold Γ_3. By left multiplying both sides of (3a) by e^T , which is a left annihilator of the control input matrix D^T, and evaluating the result on the virtual constraint manifold Γ_3, the dynamics of the snake robot on the virtual constraint manifold Γ_3 read as

$$\begin{aligned}\ddot{\theta}_N = {} & \Psi_1(\theta_N, \dot{\theta}_N, \lambda, \dot{\lambda}, \phi_0, \dot{\phi}_0, p, \dot{p}) + \\ & \Psi_2(\theta_N, \lambda, \phi_0)u_\lambda + \Psi_3(\theta_N, \lambda, \phi_0)u_{\phi_0}, \quad (16a)\\ \ddot{p} = {} & \Psi_4(\theta_N, \lambda, \phi_0)\dot{p} + \Psi_5(\theta_N, \lambda, \phi_0)\dot{\theta}_N + \\ & \Psi_6(\theta_N, \lambda, \phi_0)\dot{\lambda} + \Psi_7(\theta_N, \lambda, \phi_0)\dot{\phi}_0, \quad (16b)\\ \ddot{\phi}_0 = {} & u_{\phi_0}, \quad (16c)\\ \ddot{\lambda} = {} & u_\lambda, \quad (16d)\end{aligned}$$

where

$$\Psi_1(\cdot) = -\frac{e^T M_{\boldsymbol{\theta}} H \Phi''(\lambda)}{e^T M_{\boldsymbol{\theta}} e}\dot{\lambda}^2 - \frac{1}{e^T M_{\boldsymbol{\theta}} e}\{W_{\boldsymbol{\theta}}\dot{\boldsymbol{\theta}}^2 - lSC_{\boldsymbol{\theta}}^T f_R(\cdot)\}, \tag{17a}$$

$$\Psi_2(\cdot) = -\frac{e^T M_{\boldsymbol{\theta}} H \Phi'(\lambda)}{e^T M_{\boldsymbol{\theta}} e}, \tag{17b}$$

$$\Psi_3(\cdot) = -\frac{e^T M_{\boldsymbol{\theta}} H b}{e^T M_{\boldsymbol{\theta}} e}, \tag{17c}$$

$$\Psi_4(\cdot) = \frac{1}{Nm}E^T Q_{\boldsymbol{\theta}} E, \tag{17d}$$

$$\Psi_5(\cdot) = \frac{l}{Nm}E^T Q_{\boldsymbol{\theta}} S C_{\boldsymbol{\theta}} e, \tag{17e}$$

$$\Psi_6(\cdot) = \frac{l}{Nm}E^T Q_{\boldsymbol{\theta}} S C_{\boldsymbol{\theta}} H \Phi'(\lambda), \tag{17f}$$

$$\Psi_7(\cdot) = \frac{l}{Nm}E^T Q_{\boldsymbol{\theta}} S C_{\boldsymbol{\theta}} H b. \tag{17g}$$

In the above, each $\Psi_i(\cdot)$ is evaluated on the constraint manifold Γ_3. The equations in (16) describe a control system with two inputs, (u_λ, u_{ϕ_0}). This system completely describes the motion of the snake once the VHC (10) has been enforced. The control specification for system (16) is to stabilize θ_N to an arbitrarily small neighborhood of θ_{ref}; to stabilize $v_t = u_{\theta_N}^T \dot{p}$ to an arbitrarily small neighborhood of v_{ref}; and finally, to guarantee that $v_n = v_{\theta_N}^T \dot{p}$ converges to a neighborhood of the origin. Meanwhile, we also require $(\dot{\lambda}, \phi_0, \dot{\phi}_0)$ to remain bounded. In the process of developing controllers for the reduced dynamics system, we will require some knowledge of each $\Psi_i(\cdot)$ which is summarized in the following remark.

Remark 5.2. We make some numerical observations that are important in the subsequent development of our control laws. It can be numerically verified that for all gait parameters (α, δ): (a) $\Psi_3(\cdot) = -e^T M_{\boldsymbol{\theta}} H b / e^T M_{\boldsymbol{\theta}} e$ is bounded away from zero and negative for all $\theta_N, \lambda, \phi_0$; (b) $v_{\theta_N}^T \Psi_4(\cdot) v_{\theta_N} \approx -c_n/m$ for all $\theta_N, \lambda, \phi_0$; (c) There exists $\gamma_6 > 0$ such that $-u_{\theta_N}^T \Psi_6(\cdot) < -\gamma_6$ for all θ_N, λ and small values of ϕ_0 and for $c_n > c_t$; (d) There exists $\epsilon_0 > 0$ such that we have $|v_{\theta_N}^T \Psi_6(\cdot)| \leq \alpha\epsilon_0$ for all $\theta_N, \lambda, \phi_0$ where α denotes the amplitude of sinusoidal joint motion in (10a)–(10b); (e) $\|\Psi_4(\cdot)\| \leq c_n/m$ for all $\theta_N, \lambda, \phi_0$; (f) There exists $\gamma_7 > 0$ such that $\|\Psi_7(\cdot)\| \leq \gamma_7$ for all $\theta_N, \lambda, \phi_0$; (g) $|v_{\theta_N}^T \Psi_4(\cdot) u_{\theta_N}| < c_t/m$ for all $\theta_N, \lambda, \phi_0$. Note that the above observations are independent of the parameters N, m, l, J, because these parameters can be factored out of the Ψ_i's as it can be seen from (17). △

VI. Velocity Control

A. Head Angle Control

In this section, we use the control input u_{ϕ_0} to control the head angle of the robot in order to meet specification 2A. To this end, we consider the states $(\theta_N, \dot{\theta}_N, \phi_0, \dot{\phi}_0)$ of the constrained system (16a)-(16c). We design a high-gain feedback $u_{\phi_0}(\theta_N, \dot{\theta}_N, \phi_0, \dot{\phi}_0)$ that makes $(\theta_N - \theta_{\text{ref}}(p), \dot{\theta}_N - \dot{\theta}_{\text{ref}}(p))$ converge to an arbitrarily small neighborhood of the origin and $(\phi_0, \dot{\phi}_0)$ uniformly ultimately bounded. This analysis is made independent of the choice of u_λ, using time scale separation. By (16a) and (16c), the dynamic equations governing the states $(\theta_N, \dot{\theta}_N, \phi_0, \dot{\phi}_0)$ of the constrained system can be written as

$$\begin{aligned} \ddot{\theta}_N &= f_1(\theta_N, \dot{\theta}_N, \lambda, \dot{\lambda}, \phi_0, \dot{\phi}_0, u_\lambda) + \Psi_3(\cdot) u_{\phi_0}, \\ \ddot{\phi}_0 &= u_{\phi_0}. \end{aligned} \tag{18}$$

Proposition 6.1. *Consider the head angle control law for system* (18)

$$u_{\phi_0} = \frac{1}{\Psi_3(\cdot)}\left\{\frac{1}{\epsilon}(\dot{\tilde{\theta}}_N + k_N \tilde{\theta}_N)\right\} - k_1\phi_0 - k_2\dot{\phi}_0. \tag{19}$$

where $\tilde{\theta}_N = \theta_N - \theta_{ref}(p)$. If $u_\lambda(t), \lambda(t), \dot{\lambda}(t)$ are defined for all $t \geq 0$, then for any $k_1, k_2, \epsilon_1 > 0$, there exist $\epsilon, k_N, \epsilon_2 > 0$ and a positive definite function $V(\phi_0, \dot{\phi}_0)$ such that the set $\{(\theta_N, \dot{\theta}_N, \phi_0, \dot{\phi}_0) \,|\, \|(\tilde{\theta}_N, \dot{\tilde{\theta}}_N + k_N\tilde{\theta}_N)\| \leq \epsilon_1, V(\phi_0, \dot{\phi}_0) \leq \epsilon_2\}$ is asymptotically stable.

Remark 6.2. The result of Proposition 6.1 can be interpreted as follows. Under (19), the head angle error can be made arbitrarily small provided that ϵ is chosen to be sufficiently small. Also, ϕ_0 and $\dot{\phi}_0$ remain uniformly ultimately bounded. In the next section we define a feedback controller u_λ guaranteeing that for any initial condition, the closed-loop system has no finite escape time (see Remark 6.3). This will guarantee that the above proposition is applicable. △

Proof. Viewing the states $\lambda(t), \dot{\lambda}(t)$, and the input $u_\lambda(t)$ as exogenous signals, the control system (18) can be viewed as a time-varying system with states $(\theta_N, \dot{\theta}_N, \phi_0, \dot{\phi}_0)$. Under the control input (19), the closed-loop dynamics of system (18) in the standard singular perturbation form become

$$\begin{aligned} &\dot{\tilde{\theta}}_N = \tilde{\omega}_N, \\ &\epsilon\dot{\tilde{\omega}}_N = \epsilon[\ddot{\theta}_{\text{ref}} + g_1(t, \phi_0, \dot{\phi}_0, \theta_N, \dot{\theta}_N) + \\ &\Psi_3(\cdot)(k_1\phi_0 + k_2\dot{\phi}_0)] \\ &-(\tilde{\omega}_N + k_N\tilde{\theta}_N), \end{aligned} \tag{20}$$

where

$$g_1(t, \phi_0, \dot{\phi}_0, \theta_N, \dot{\theta}_N) = f_1(\theta_N, \dot{\theta}_N, \lambda(t), \dot{\lambda}(t), \phi_0, \dot{\phi}_0, u_\lambda(t)).$$

Here we use time-scale separation to make the analysis independent of the choice of u_λ. Note that (20) is a singularly perturbed system with reduced dynamics

$$\dot{\tilde{\theta}}_N = -k_N\tilde{\theta}_N, \tag{21}$$

and boundary-layer dynamics

$$\frac{d\hat{y}}{d\tau} = -\hat{y}, \tag{22}$$

where $\hat{y} = \tilde{\omega}_N + k_N\tilde{\theta}_N$. The origin is an exponentially stable equilibrium point of the reduced system. Also, the origin is an exponentially stable equilibrium point of the boundary-layer system. According to the singular perturbation theorem on an infinite interval (see Theorem 11.2 in [33]), for all $\tilde{\theta}_N(0) \in \Re$

and $t_0 \geq 0$, the singularly perturbed system (20) has a unique solution $(\tilde{\theta}_N(t,\epsilon), \tilde{\omega}_N(t,\epsilon))$ such that

$$\begin{aligned} &\tilde{\theta}_N(t,\epsilon) - \exp(-k_N(t-t_0))\tilde{\theta}_N(0) \\ &= O(\epsilon), \qquad (23a) \\ &\tilde{\omega}_N(t,\epsilon) + k_N \exp(-k_N(t-t_0))\tilde{\theta}_N(0) \\ &- \exp(-\frac{t}{\epsilon})y_0 = O(\epsilon), \qquad (23b) \end{aligned}$$

for all $t \in (0,\infty)$. Note that the closed-loop dynamics governing the states $(\phi_0, \dot{\phi}_0)$ become

$$\ddot{\phi}_0 + k_2\dot{\phi}_0 + k_1\phi_0 = \underbrace{\frac{1}{\Psi_3(\cdot)}\left\{\frac{1}{\epsilon}(\dot{\tilde{\theta}}_N + k_N\tilde{\theta}_N)\right\}}_{f_N(t,\epsilon)}. \tag{24}$$

From (23a)–(23b), it can be seen that $f_N(t,\epsilon)$ is uniformly bounded and of order $O(1)$, i.e., there exist positive constants k_0 and c_0 such that $|f_N(t,\epsilon)| \leq k_0$ for all $|\epsilon| < c_0$. Since the unforced system $\ddot{\phi}_0 + k_2\dot{\phi}_0 + k_1\phi_0 = 0$ is an LTI system and has a globally exponentially stable equilibrium point at the origin $(\phi_0, \dot{\phi}_0) = (0,0)$, the system (24) is input-to-state stable. Therefore, there exists an ISS-Lyapunov function $V(.)$ and ϵ_2 such that the set $\{V(\phi_0, \dot{\phi}_0) \leq \epsilon_2\}$ is asymptotically stable (see Theorem 10.4.1 in [34]). Now, we consider the change of variable $\hat{y} = \tilde{\omega}_N + k_N\tilde{\theta}_N$. The closed-loop dynamics become

$$\begin{aligned} &\dot{\tilde{\theta}}_N = \hat{y} - k_N\tilde{\theta}_N, \\ &\epsilon\dot{\hat{y}} = \epsilon[\ddot{\theta}_{\text{ref}} + g_1(t,\phi_0,\dot{\phi}_0,\theta_N,\dot{\theta}_N) + \\ &\Psi_3(\cdot)(k_1\phi_0 + k_2\dot{\phi}_0) + k_N(\hat{y} - k_N\tilde{\theta}_N)] - \hat{y}, \end{aligned} \tag{25}$$

Next,we consider the Lyapunov function candidate $V_1 = (1/2)\tilde{\theta}_N^2 + (1/2)\hat{y}^2$. We have

$$\dot{V}_1 = \tilde{\theta}_N\hat{y} - k_N\tilde{\theta}_N^2 + \hat{y}\dot{\hat{y}} \tag{26}$$

It can be shown that there exists $L_3 > 0$ such that $\hat{y}\dot{\hat{y}} \leq -(1/2\epsilon)\hat{y}^2 + L_3\hat{y}$ (see proof of Theorem 11.1 in [33]). We have

$$\dot{V}_1 \leq \tilde{\theta}_N\hat{y} - k_N\tilde{\theta}_N^2 - \frac{1}{2\epsilon}\hat{y}^2 + L_3\hat{y} \tag{27}$$

Completing the squares, we get

$$\dot{V}_1 \leq -(k_N - \frac{1}{2})\tilde{\theta}_N^2 - (\frac{1}{2\epsilon} - 1)\hat{y}^2 + \frac{1}{2}L_3^2 \tag{28}$$

For $k_N > (1/2)(L_3^2/4\epsilon_1^2 + 1)$ and $\epsilon < 1/(L_3^2/4\epsilon_1^2 + 2)$ we have

$$\dot{V}_1 \leq -\frac{L_3^2}{4\epsilon_1^2}V + \frac{1}{2}L_3^2 \tag{29}$$

By the comparison lemma [33], we get

$$V_1(t) \leq V_1(0)\exp(-\frac{L_3^2}{4\epsilon_1^2}t) + 2\epsilon_1^2 \tag{30}$$

This implies that $\|[\tilde{\theta}_N, \hat{y}]^T\|$ converges to a neighborhood of the origin given by ϵ_1. Therefore, the set $\{\|[\tilde{\theta}_N, \hat{y}]^T\| \leq \epsilon_1\}$ is asymptotically stable. Note that ϵ_1 is a design parameter that we can choose arbitrarily.

□

B. Speed Control

We now turn our attention to specification 2B. Consider the reduced dynamics (16). In the previous section, we controlled the states $\theta_N, \dot{\theta}_N, \phi_0, \dot{\phi}_0$. Now, we are left with the states $p, \dot{p}, \lambda, \dot{\lambda}$. The map $\dot{p} \mapsto (v_t, v_n)$ is a diffeomorphism so for velocity control we may consider the subsystem with states $(\Delta v_t, v_n, \lambda, \dot{\lambda})$, with $\Delta v_t = v_t - v_{\text{ref}}(p)$. In order to obtain the tangential and normal velocity dynamics evaluated on the constraint manifold, we take the time derivatives of Equations (7a), (7b), which using (16b) yields

$$\begin{aligned} \dot{v}_t = \quad & u_{\theta_N}^T\Psi_4(\cdot)u_{\theta_N}v_t + u_{\theta_N}^T\Psi_4(\cdot)v_{\theta_N}v_n + \dot{\theta}_N v_n + \\ & u_{\theta_N}^T\Psi_5(\cdot)\dot{\theta}_N + u_{\theta_N}^T\Psi_6(\cdot)\dot{\lambda} + u_{\theta_N}^T\Psi_7(\cdot)\dot{\phi}_0 \quad (31a) \\ \dot{v}_n = \quad & v_{\theta_N}^T\Psi_4(\cdot)u_{\theta_N}v_t + v_{\theta_N}^T\Psi_4(\cdot)v_{\theta_N}v_n - \dot{\theta}_N v_t + \\ & v_{\theta_N}^T\Psi_5(\cdot)\dot{\theta}_N + v_{\theta_N}^T\Psi_6(\cdot)\dot{\lambda} + v_{\theta_N}^T\Psi_7(\cdot)\dot{\phi}_0. \quad (31b) \end{aligned}$$

Thus, the velocity error dynamics have the form

$$\begin{aligned} \Delta\dot{v}_t = \quad & f_2(\theta_N, \dot{\theta}_N, \lambda, \phi_0, \dot{\phi}_0, \Delta v_t, v_n) + \\ & u_{\theta_N}^T\Psi_6(\cdot)\dot{\lambda} - (dv_{\text{ref}})_p\dot{p}, \qquad (32a) \\ \dot{v}_n = \quad & f_3(\theta_N, \dot{\theta}_N, \lambda, \dot{\lambda}, \phi_0, \dot{\phi}_0, \Delta v_t, v_n) + \\ & v_{\theta_N}^T\Psi_4(\cdot)v_{\theta_N}v_n, \qquad (32b) \\ \ddot{\lambda} = \quad & u_\lambda. \qquad (32c) \end{aligned}$$

In order to stabilize the solutions of (32a), (32b) to a neighborhood of the origin, we use the following control input

$$\begin{aligned} u_\lambda = & -K_z(\dot{\lambda} + K_\lambda\Delta v_t) \\ & - K_\lambda[f_2(\cdot) + u_{\theta_N}^T\Psi_6(\cdot)\dot{\lambda} - (dv_{\text{ref}})_p\dot{p}]. \end{aligned} \tag{33}$$

where $K_\lambda > 0$ and $K_z > 0$ are positive constants. Note that $u_{\theta_N}^T\Psi_6(\cdot)$ is bounded away from zero by part (c) of Remark 5.2 provided that the ultimate bound on ϕ_0 from Proposition 6.1 is small enough.

Remark 6.3. Consider the state vector $x = [v_t, v_n, \lambda, \dot{\lambda}, \phi_0, \dot{\phi}_0]^T$. Under the control laws (19) and (33), we have $\dot{x} = f(x)$ for the closed loop system. Because of the uniform bounds on $\Psi_i, i = 2, \ldots, 7$, it can be seen that $\|f(x)\| \leq B(1 + \|x\|)$ for some constant B. Because of this linear growth condition, there is no finite escape time and the signals $\dot{\lambda}(t), u_\lambda(t)$ are defined for all $t \geq 0$ as required by Proposition 6.1. △

We have the following proposition regarding the forward velocity control system.

Proposition 6.4. *Consider the control system* (32a)-(32c) *under the controller* (33) *with $c_n > c_t$. If the ultimate bound* *on ϕ_0 from Proposition 6.1 is small enough that $u_{\theta_N}^T \Psi_6(\cdot)$ is bounded away from zero, then for all $\epsilon_3 > 0$ and for sufficiently large controller gain $K_\lambda > 0$, there exists $\epsilon_4 > 0$ such that the compact set $\Lambda_1 = \{(\lambda, \dot{\lambda}, \Delta v_t, v_n) : |\Delta v_t| \leq \epsilon_3, \dot{\lambda} = -K_\lambda \Delta v_t, |v_n| \leq \epsilon_4\}$ is asymptotically stable.*

Remark 6.5. The result of Proposition 6.4 can be interpreted as follows. Under (33), the velocity error Δv_t can be made arbitrarily small provided that the gain K_λ is chosen to be sufficiently large. Also, the normal velocity v_n remains uniformly ultimately bounded. △

Proof. The control law (33) is a feedback linearizing controller for system (32a) with output $z = \dot{\lambda} + K_\lambda \Delta v_t$, and it makes the set $\Lambda_3 = \{(\lambda, \dot{\lambda}, \Delta v_t, v_n) : \dot{\lambda} = -K_\lambda \Delta v_t\}$ asymptotically stable. On the set Λ_3, the subsystem (32a) becomes

$$\Delta \dot{v}_t = f_2(\cdot) - K_\lambda u_{\theta_N}^T \Psi_6(\cdot) \Delta v_t - (dv_{\text{ref}})_p \dot{p} \tag{34}$$

Now, we find a positively invariant set

$$\Omega = \{(\lambda, \dot{\lambda}, \Delta v_t, v_n) : |\Delta v_t| \leq \bar{V}_1,\ |v_n| \leq \bar{V}_2\}, \tag{35}$$

such that $|f_2(\theta_N, \dot{\theta}_N, \lambda, \phi_0, \dot{\phi}_0, \Delta v_t, v_n)|$ is uniformly bounded on Ω. Note that ϕ_0, $\dot{\phi}_0$ have been proven to be uniformly ultimately bounded in Proposition 6.1. Therefore we need to show boundedness of Δv_t, v_n. We pick $\bar{V}_1$ arbitrary and determine K_3 such that $|f_3(\cdot)| \leq K_3$. Note that K_3 depends on $\bar{V}_1$. Next, we pick $\bar{V}_2 > K_3/K_n$. Finally, we choose

$$K_\lambda > \frac{K_1 + K_2 \bar{V}_2}{\gamma_6 \bar{V}_1}. \tag{36}$$

We claim that Ω is positively invariant. Note that

$$\begin{aligned} -K_\lambda \gamma_6 \Delta v_t - K_1 - K_2 |v_n| \leq \Delta \dot{v}_t \leq -K_\lambda \gamma_6 \Delta v_t \\ -K_1 + K_2 |v_n|, \end{aligned} \tag{37}$$

and

$$-K_n v_n - K_3 \leq \dot{v}_n \leq -K_n v_n + K_3. \tag{38}$$

On $\Delta v_t = \bar{V}_1$, we have $\Delta \dot{v}_t \leq -K_\lambda \gamma_6 \bar{V}_1 + K_1 + K_2 |v_n| \leq -K_\lambda \gamma_6 \bar{V}_1 + K_1 + K_2 \bar{V}_2 \leq 0$. On $\Delta v_t = -\bar{V}_1$, we have $\Delta \dot{v}_t \geq K_\lambda \gamma_6 \bar{V}_1 - K_1 - K_2 |v_n| \geq K_\lambda \gamma_6 \bar{V}_1 - K_1 - K_2 \bar{V}_2 \geq 0$. On $v_n = \bar{V}_2$, we have $\dot{v}_n \leq -K_n \bar{V}_2 + K_3 \leq 0$. On $v_n = -\bar{V}_2$, we have $\dot{v}_n \geq K_n \bar{V}_2 - K_3 \geq 0$. The inequalities above prove that on $\partial\Omega$, the vector field given by (32a)–(32b) points inside Ω. Therefore, by Nagumo's theorem [35], the set Ω is positively invariant. For all initial conditions in Ω, we have $|f_2(\cdot)| \leq \gamma_2 = K_1 + K_2 \bar{V}_2$. Now, we employ the Lyapunov function candidate $V_1 = \frac{1}{2}\Delta v_t^2$, we have $\dot{V}_1 < -K_\lambda \gamma_6 \Delta v_t^2 + \gamma_2 \Delta v_t$. Therefore we have

$$\dot{V}_1 < -(K_\lambda \gamma_6 - \frac{1}{2}) \Delta v_t^2 + \frac{1}{2}\gamma_2^2 \tag{39}$$

Using the comparison lemma [33], we have, for all $t \geq 0$

$$V_1(t) \leq \exp(-(K_\lambda \gamma_6 - \frac{1}{2})t) V_1(0) + \frac{1}{2(K_\lambda \gamma_6 - \frac{1}{2})} \gamma_2^2 \tag{40}$$

Therefore, Δv_t converges to a ball of radius $\sqrt{\gamma_2^2/(K_\lambda \gamma_6 - \frac{1}{2})}$. Choosing K_λ large enough makes the ultimate bound of Δv_t less than ϵ_3 for any desired $\epsilon_3 > 0$. Letting $\epsilon_3 = \sqrt{\gamma_2^2/(K_\lambda \gamma_6 - \frac{1}{2})}$, the set $\Lambda_2 = \{(\lambda, \dot{\lambda}, \Delta v_t, v_n) \in \Lambda_3 : |\Delta v_t| \leq \epsilon_3\}$ is asymptotically stable relative to Λ_3. On the set Λ_2, the dynamics are described by subsystem (32b). The function $f_3(\cdot)$ is uniformly bounded on Λ_2, namely, there exists $\gamma_3 > 0$ such that $|f_3(\cdot)| \leq \gamma_3$ on Λ_2. Employing the Lyapunov function candidate $V_2 = 1/2 v_n^2$ and using part (b) of Remark 5.2 yields

$$\begin{aligned} \dot{V}_2 \leq \frac{-c_n}{m} v_n^2 + \gamma_3 v_n \leq -\frac{c_n}{m} v_n^2 + \\ \frac{\gamma}{2} v_n^2 + \frac{1}{2\gamma}\gamma_3^2, \end{aligned} \tag{41}$$

where γ is some positive constant and we have used Young's inequality, $ab \leq (\gamma/2)a^2 + (1/2\gamma)b^2$. We conclude that there exists a sufficiently small positive constant β such that

$$\dot{V}_2 \leq -\beta V_2 + \frac{1}{2\gamma}\gamma_3^2. \tag{42}$$

Using the comparison lemma [33], we have, for all $t \geq 0$,

$$V_2(t) \leq \exp(-\beta t) V_2(0) + \frac{1}{2\gamma\beta}\gamma_3^2. \tag{43}$$

Therefore, v_n converges to a ball of radius $\sqrt{\gamma_3^2/(\gamma\beta)}$. Letting $\epsilon_4 = \sqrt{\gamma_3^2/(\gamma\beta)}$, the set $\Lambda_1 = \{(\lambda, \dot{\lambda}, \Delta v_t, v_n) \in \Lambda_2 : |v_n| \leq \epsilon_4\}$ is asymptotically stable relative to Λ_2. This set is compact because $\lambda \in S^1$, which is a compact set and on Λ_1, $|\Delta v_t| \leq \epsilon_3$, and $\dot{\lambda} = -K_\lambda \Delta v_t$. In the above analysis, $\Lambda_1 \subset \Lambda_2 \subset \Lambda_3$. Also, Λ_i is asymptotically stable relative to Λ_{i+1} for the closed-loop system for $i = 1, 2$. On the other hand, Λ_1 is a compact set. Using Proposition 2.2, we conclude that the set Λ_1 is asymptotically stable. □

VII. Path Following Control of Snake Robots

In this section we carry out the last design stage: the path following control. Thus far we have developed a velocity controller that asymptotically stabilizes the direction following manifold

$$\begin{aligned} \Gamma_2 = \{(\boldsymbol{\theta}, \dot{\boldsymbol{\theta}}, p, \dot{p}, \lambda, \dot{\lambda}, \phi_0, \dot{\phi}_0) \in \Gamma_3 : \\ \|(\tilde{\theta}_N, \dot{\tilde{\theta}}_N + k_N \tilde{\theta}_N)\| \leq \epsilon_1, V(\phi_0, \dot{\phi}_0) \leq \epsilon_2 \\ |v_t - v_{\text{ref}}(p)| \leq \epsilon_3, |v_n| \leq \epsilon_4, \dot{\lambda} = -K_\lambda \Delta v_t\}. \end{aligned} \tag{44}$$

The next objective is to design $\theta_{\text{ref}}(p)$ and $v_{\text{ref}}(p)$ in (9) to stabilize an arbitrary small neighborhood of the planar curve $\{h(p) = 0\}$ while regulating the velocity along the curve. To this end, we define the path following manifold as follows

$$\Gamma_1 = \{(\boldsymbol{\theta}, \dot{\boldsymbol{\theta}}, p, \dot{p}, \lambda, \dot{\lambda}, \phi_0, \dot{\phi}_0) \in \Gamma_2 : |h(p)| \leq \epsilon_5\}, \quad (45)$$

where ϵ_5 is a small constant.

Remark 7.1. The set Γ_1 is compact. The reason is that the inequality $|h(p)| \leq \epsilon_5$ implies that p is bounded because $h(\cdot)$ is a continuous function. Since $\theta_{\text{ref}}(\cdot)$ and $v_{\text{ref}}(\cdot)$ are continuous functions, $\theta_{\text{ref}}(p)$ and $v_{\text{ref}}(p)$ are bounded. Therefore, θ_N and v_t are bounded. Since v_t and v_n are bounded, $\dot{p}$ is bounded. Since θ_N and ϕ_0 are bounded and $\boldsymbol{\theta} = e\theta_N + H\Phi(\lambda) + Hb\phi_0$ on the set Γ_1, $\boldsymbol{\theta}$ is bounded. Since $\dot{\boldsymbol{\theta}} = e\dot{\theta}_N + H\Phi^{'}(\lambda)\dot{\lambda} + Hb\dot{\phi}_0$, and $\dot{\theta}_N$, $\dot{\lambda}$, and $\dot{\phi}_0$ are bounded, $\dot{\boldsymbol{\theta}}$ is bounded. △

Recalling that $\mu(p) = [v_{\text{ref}}(p)\cos(\theta_{\text{ref}}(p)), v_{\text{ref}}(p)\sin(\theta_{\text{ref}}(p))]^T$, we have the following lemma:

Lemma 7.2. *Let $\Delta_1 = \theta_N - \theta_{ref}(p)$. We have the following relationship between the velocity vector of the center of mass $\dot{p}$ and the reference velocity vector $\mu(p)$:*

$$\dot{p} = R_{\Delta_1}\mu(p) + d(v_t, v_n, \theta_N, v_{ref}(p)), \quad (46)$$

where $\|d(\cdot)\| \leq \epsilon_3 + \epsilon_4$ on the direction following manifold Γ_2.

Proof. Applying the operator $\mathfrak{C}$ to the vector $\dot{p} - R_{\Delta_1}\mu(p)$, we have

$$\begin{aligned}&\mathfrak{C}(\dot{p} - R_{\Delta_1}\mu(p)) \underbrace{=}_{\text{Equation (8)}} \mathfrak{C}\bigg(R_{\theta_N}\begin{bmatrix} v_t \\ v_n \end{bmatrix} \\ &-v_{\text{ref}}(p)R_{\Delta_1}\begin{bmatrix} \cos(\theta_{\text{ref}}(p)) \\ \sin(\theta_{\text{ref}}(p)) \end{bmatrix}\bigg) \underbrace{=}_{\text{Lemma 2.4}} \\ &\exp(j\theta_N)(v_t + jv_n) - v_{\text{ref}}(p)\underbrace{\exp(j\Delta_1)\exp(j\theta_{\text{ref}}(p))}_{\exp(j\theta_N)}.\end{aligned}$$

Applying $\mathfrak{C}^{-1}$ to both sides of the above equality, we have

$$\dot{p} - R_{\Delta_1}\mu(p) = \underbrace{R_{\theta_N}\begin{bmatrix} v_t - v_{\text{ref}}(p) \\ v_n \end{bmatrix}}_{d(v_t, v_n, \theta_N, v_{\text{ref}}(p))}.$$

Therefore, we have $\|d(.)\| \leq \sqrt{(v_t - v_{\text{ref}}(p))^2 + v_n^2}$. On the direction following manifold Γ_2, we have $|v_t - v_{\text{ref}}(p)| < \epsilon_2$ and $|v_n| < \epsilon_3$. It follows that $\|d(.)\| \leq \epsilon_2 + \epsilon_3$. □

If we let $y = h(p)$, we want $y \to 0$ to meet specification (i) of the PFP. On the direction following manifold Γ_2, we have

$$\dot{y} = dh_p\dot{p} = dh_pR_{\Delta_1}\mu + dh_pd(\cdot) \quad (47)$$

We propose to use the following control law for determining the reference velocity

$$\mu(p) = \underbrace{-\frac{dh_p^T}{\|dh_p\|^2}K_{\text{tran}}h(p)}_{\mu^{\perp}(p)} + \underbrace{\begin{bmatrix} 0 & 1 \\ -1 & 0 \end{bmatrix} dh_p^T\frac{v}{\|dh_p\|}}_{\mu^{\|}(p)} \quad (48)$$

where K_{tran} is a positive constant.

Remark 7.3. Since $dh_p^T = \nabla h(p)$ is perpendicular to the level sets of $h(\cdot)$, the control law (48) can be intuitively described as follows. The reference velocity $\mu(p)$ is composed of two components: (a) the component $\mu^{\perp}(p)$ is perpendicular to the level sets of $h(\cdot)$ and decreases the distance of the center of mass to the curve $\gamma = h^{-1}(0)$; (b) the component $\mu^{\|}(p)$ is tangent to the level sets of $h(\cdot)$ and regulates the velocity of the center of mass on the curve $\gamma = h^{-1}(0)$. △

We have the following proposition regarding the path following controller.

Proposition 7.4. *Consider system* (47) *where $|\Delta_1| < \epsilon_1$. For sufficiently small ϵ_1 the following property holds: for any $\epsilon_5 > 0$ there exists K_{tran} such that the set $\{|h(p)| \leq \epsilon_5\}$ is asymptotically stable for* (47)*. Moreover, the velocity control specification, i.e., $\|\dot{p}\| = v$, is approximately met on γ: $\big|\|\dot{p}\| - v\big| \leq \epsilon_3 + \epsilon_4$.*

Proof. Using the control input (48) in (47) the closed loop equation is obtained as follows

$$\begin{aligned}&\dot{y} = -\frac{dh_pR_{\Delta_1}dh_p^T}{\|dh_p\|^2}K_{\text{tran}}y + \\ &dh_pR_{\Delta_1}\begin{bmatrix} 0 & 1 \\ -1 & 0 \end{bmatrix}dh_p^T\frac{v}{\|dh_p\|} + dh_pd(\cdot) \quad (49)\end{aligned}$$

Now, we consider the Lyapunov function candidate $V = \frac{1}{2}y^2$. We pick $c > 0$ and define $\Omega_c = \{|y| \leq c\}$. By assumption, on $\{p : h(p) = 0\}$ it holds that $dh_p \neq [0 \;\; 0]$. Therefore, there exists $c > 0$ such that $dh_p \neq 0$ for all $p \in \{p : |h(p)| \leq c\}$. Let $\Omega_c = \{p : |h(p)| \leq c\}$. We will now show that for sufficiently large K_{tran}, Ω_c is positively invariant. To this end, it is enough to show that there exists $K^\star > 0$ such that for all $K_{\text{tran}} \geq K^\star$, $\dot{V} \leq 0$ for all $p \in \partial\Omega_c$. On $\partial\Omega_c$, dh_p is bounded. Therefore, $|dh_pd(\cdot)| \leq K$. By continuity, for small enough ϵ_1 (note that ϵ_1 can be made arbitrarily small by Proposition 6.1), there exist $a_1, a_2 > 0$ such that

$$-\frac{dh_pR_{\Delta_1}dh_p^T}{\|dh_p\|^2} \leq -a_1, \quad (50)$$

and

$$|dh_pR_{\Delta_1}\begin{bmatrix} 0 & 1 \\ -1 & 0 \end{bmatrix}dh_p^T\frac{v}{\|dh_p\|}| \leq a_2 \quad (51)$$

We have

$$\begin{aligned}&\dot{V} = y\dot{y} \leq -K_{\text{tran}}a_1y^2 + a_2y + dh_pd(\cdot)y \leq \\ &-K_{\text{tran}}c^2 + a_2|c| + K|c| \quad (52)\end{aligned}$$

Therefore, if $K_{\text{tran}} \geq \frac{a_2+K}{|c|}$, we get $\dot{V} \leq 0$ on $\partial\Omega_c$. This means that Ω_c is positively invariant. On Ω_c, we have $|dh_pd(\cdot)| \leq K_c$ because Ω_c is compact. Therefore, we get

$$\begin{aligned}\dot{V} &\leq -K_{\text{tran}} a_1 y^2 + (K_c + a_2)|y| \leq \\ &-K_{\text{tran}} y^2 + \frac{1}{2} y^2 + \frac{1}{2}(K_c + a_2)^2 \implies \\ \dot{V} &\leq -(K_{\text{tran}} - \frac{1}{2}) y^2 + \frac{1}{2}(K_c + a_2)^2 \end{aligned} \tag{53}$$

Therefore for $K_{\text{tran}} \geq \frac{1}{2}$, we have (by the comparison lemma)

$$V(t) \leq \exp((-K_{\text{tran}} + \frac{1}{2})t)V(0) + \frac{\frac{1}{2}(K_c + a_2)^2}{K_{\text{tran}} - \frac{1}{2}} \tag{54}$$

Therefore, y converges to a ball of radius $\sqrt{\frac{\frac{1}{2}(K_c+a_2)^2}{K_{\text{tran}}-\frac{1}{2}}}$. Choosing K_{tran} large enough makes the ultimate bound of y less than ϵ_5 for any desired $\epsilon_5 > 0$. Therefore, the path γ is practically stable with domain of attraction containing Ω_c. On the path γ, $h(p) = 0$, and we have

$$\dot{p} = R_{\Delta_1} \begin{bmatrix} 0 & 1 \\ -1 & 0 \end{bmatrix} dh_p^T \frac{v}{\|dh_p\|} + d(\cdot) \tag{55}$$

Therefore, we have

$$v - \|d(\cdot)\| \leq \|\dot{p}\| \leq v + \|d(\cdot)\| \implies \big|\, \|\dot{p}\| - v \big| \leq \|d(\cdot)\| \leq \epsilon_3 + \epsilon_4 \tag{56}$$

Therefore, we have approximate velocity control on γ.

□

VIII. Main Result

For the snake robot model (3a)–(3b), we proposed the following control law

$$\begin{aligned} u = &(DM_{\boldsymbol{\theta}}^{-1}D^T)^{-1}\{DM_{\boldsymbol{\theta}}^{-1}W_{\boldsymbol{\theta}}\dot{\boldsymbol{\theta}}^2 \\ &-lDM_{\boldsymbol{\theta}}^{-1}SC_{\boldsymbol{\theta}}^T f_R + \Phi''(\lambda)\dot{\lambda}^2 + \Phi'(\lambda)u_\lambda \\ &+bu_{\phi_0} - K_P[D\boldsymbol{\theta} - \Phi(\lambda) - b\phi_0] \\ &-K_D[D\dot{\boldsymbol{\theta}} - \Phi'(\lambda)\dot{\lambda} - b\dot{\phi}_0]\}, \end{aligned} \tag{57}$$

where ϕ_0, $\dot{\phi}_0$, λ, and $\dot{\lambda}$ are the states of the following dynamic compensators

$$\ddot{\lambda} = u_\lambda, \ \ddot{\phi}_0 = u_{\phi_0}, \tag{58}$$

and the control input u_{ϕ_0} is given by

$$u_{\phi_0} = \frac{1}{\Psi_3(\cdot)} \left\{ \frac{1}{\epsilon}(\dot{\tilde{\theta}}_N + k_N \tilde{\theta}_N) \right\} - k_1\phi_0 - k_2\dot{\phi}_0, \tag{59}$$

where $\tilde{\theta}_N = \theta_N - \theta_{\text{ref}}(p)$. Also, the control input u_λ is given by

$$\begin{aligned} u_\lambda = &-K_z(\dot{\lambda} + K_\lambda \Delta v_t) \\ &- K_\lambda[f_2(\cdot) + u_{\theta_N}^T \Psi_6(\cdot)\dot{\lambda} - (dv_{\text{ref}})_p \dot{p}], \end{aligned} \tag{60}$$

where $K_\lambda > 0$ and $K_z > 0$ are positive constants. The reference signals $\theta_{\text{ref}}(p)$ and $v_{\text{ref}}(p)$ in (59) and (60) are determined from the identity $\mu(p) = v_{\text{ref}}(p)[\cos(\theta_{\text{ref}}(p)), \sin(\theta_{\text{ref}}(p))]$ where $\mu(p)$ is given by

$$\mu(p) = -\frac{dh_p^T}{\|dh_p\|^2} K_{\text{tran}} h(p) + \begin{bmatrix} 0 & 1 \\ -1 & 0 \end{bmatrix} dh_p^T \frac{v}{\|dh_p\|} \tag{61}$$

where K_{tran} is a positive constant. We have

$$\theta_{\text{ref}}(p) = \text{atan}(\mu_1(p), \mu_2(p)), \tag{62}$$

$$v_{\text{ref}}(p) = \|\mu(p)\|. \tag{63}$$

Note that $\mu(p) = [v_{\text{ref}}(p)\cos(\theta_{\text{ref}}(p)),\ v_{\text{ref}}(p)\sin(\theta_{\text{ref}}(p))]$, i.e., $\theta_{\text{ref}}(p)$ and $v_{\text{ref}}(p)$ are generated according to Equations (62) and (63) where $\mu(p)$ is determined using (61). We have the following theorem regarding the snake robot control system.

Theorem 8.1 (**Main Result).** *Consider the snake robot model* (3a)–(3b) *with feedback* (57), (59), (60), *and* (61). *Suppose that the ultimate bound on ϕ_0 from Proposition 6.1 is small enough such that $u_{\theta_N}^T \Psi_6(\cdot)$ is bounded away from zero. For any $\epsilon_5 > 0$, there exist a sufficiently small ϵ in* (59)*, a sufficiently large K_λ in* (60) *and K_{tran} in* (61) *such that the path following manifold Γ_1 in* (45) *is asymptotically stable and the velocity of the snake robot satisfies the asymptotic bound* $\limsup \big|\, \|\dot{p}\| - v\big| \leq \epsilon_3 + \epsilon_4$.

Proof. Consider the sets Γ_1, Γ_2, Γ_3 defined in (45), (44), (14) and note that $\Gamma_1 \subset \Gamma_2 \subset \Gamma_3$. Also, by Proposition 7.4, Γ_1 is asymptotically stable relative to Γ_2 and by Propositions 6.1 and 6.4, Γ_2 is asymptotically stable relative to Γ_3 for the closed-loop system. On the other hand, Γ_1 is a compact set (see Remark 7.1). Using Proposition 2.2, we conclude that the set Γ_1 is asymptotically stable. □

IX. Simulation Results

Simulation parameters. In this section, we present the simulation results which illustrate the performance of the proposed path following controller. We consider a snake robot with $N = 10$ links with length $2l = 0.14$ m, mass $m = 1$ kg, and moment of inertia $J = 0.0016$ kg.m^2. The friction coefficients are $c_t = 0.5$ and $c_n = 3$. The parameters of the VHC are chosen to be $\alpha = 30\pi/180$ rad, and $\delta = 72\pi/180$ rad. The model parameters are chosen based on the snake robot Wheeko in the NTNU snake robotics laboratory.

Circle tracking. We would like to follow a circular path with radius 2 m. The initial conditions are $\theta(0) = [0, \ldots, 0]^T$, $\dot{\theta}(0) = [0, \ldots, 0]^T$, $p(0) = [-4, 1]^T$, $\dot{p}(0) = [0, 0]^T$, $\lambda(0) = \dot{\lambda}(0) = \phi(0) = \dot{\phi}(0) = 0$. We run the simulation for 600 seconds. The controller parameters are listed in Table II. Note that ϵ determines the ultimate bound on head angle error. Also, k_N determines the rate of convergence of θ_N to θ_{ref}. The gains k_1 and k_2 have influence on the ultimate bound of ϕ_0. The gains K_λ and K_z determine the rate of convergence and ultimate bound of Δv_t. Finally, K_{tran} controls the path following error. In order to show the performance of the proposed control scheme in the presence of angular position measurement noise, we subject every i^{th} link angle θ_i to an additive noise by using Matlab function `randn()`

which generates normally distributed pseudorandom numbers that can be considered as measurement noise for the joint angles. The root mean square (RMS) of the noise applied to the joint angle measurements was 0.1 rad.

The simulation results show that the snake robot follows the desired path while the states of the compensators in (11) remain uniformly ultimately bounded. Figure 3 depicts the snake robot and the trajectory of the center of mass of the robot. Figure 4 depicts the path following error. The RMS value of the path following error in the steady state is 0.12 m. Figure 5 depicts the dynamic variable ϕ_0. As it is shown in Theorem 8.1, the variable ϕ_0 remains uniformly ultimately bounded. Figure 6 depicts the dynamic variable $\dot{\lambda}$, and thus gives the frequency of the undulatory motion. This is within acceptable range of frequency of oscillations of the existing snake robots at the NTNU snake robotics laboratory (up to 2 rad/sec). Figure 7 depicts the shape variable error. As it can be seen from the figure, the error converges exponentially to the origin. Figure 8 depicts the actual and the reference tangential velocities. The reason for the steady state error is that the gain K_λ in control law (33) is not large enough. Choosing K_λ sufficiently large causes the velocity error Δv_t to become arbitrarily small. However, such large gain values cause large oscillations and large control torques. Figure 9 depicts the head angle tracking error. As it is shown in Theorem 8.1, the tracking error remains uniformly ultimately bounded. Finally, Figure 10 depicts the norm of the control torque vector, from which we can see that the control torques are within the physical limitations/saturation values of the existing snake robots at the NTNU snake robotics laboratory (up to 7 Nm).

As it can be seen from (48), when the path following error $\|h(p)\|$ is large, the reference speed $\|\mu(p)\| = v_{\text{ref}}(p)$ will be large. Tracking such a large reference speed will require very fast oscillations of the snake robot and large control torques. In order to avoid such large initial oscillations and joint control torques, if $\|h(p)\| > 0.4$ we set $v_{\text{ref}}(p) = 0.05$ m/sec. If $\|h(p)\| < 0.3$, we set $v_{\text{ref}}(p) = \|\mu(p)\|$ where $\mu(p)$ is determined from (46). Finally if $0.3 \leq \|h(p)\| \leq 0.4$, we let the reference speed be determined from the smooth interpolation between 0.05 and $\|\mu(p)\|$, i.e., from $(0.5 - 10\|\mu(p)\|)\|h(p)\| + (4\|\mu(p)\| - 0.15)$.

TABLE II
CONTROLLER PARAMETERS

Controller parameter	Controller expression	Numerical values in simulations
K_P	(15)	$10I_2$
K_D	(15)	$10I_2$
ϵ	(19)	10^{-1}
k_N	(19)	10
k_1	(19)	1
k_2	(19)	1
K_z	(33)	50
K_λ	(33)	50
K_{tran}	(48)	0.6
v	(48)	0.05

Remark 9.1. According to Equation (15), the magnitude of the control torque input depends on u_{ϕ_0}. According to Equation (19), the magnitude of u_{ϕ_0} depends on the head angle error. Therefore, if we have large head angle errors, large joint torques will be applied to the body. However, we can saturate the exceedingly large torques and use anti-windup design for our robotic system [36]. $\triangle$

Remark 9.2. **(Control Algorithm Computational Time)** We implemented the controller using Matlab R2012a on a MacBook Pro with CPU 2.9 GHz Intel Core i7 and 8 GB of RAM. We used `ode1()`, which implements the forward Euler method of order 1 (a non-adaptive method), in order to measure how long it takes to compute the control law using a fixed step size ode solver. According to our results, it takes 0.0026 seconds for the control law to be computed at each time step of length 1 ms for a snake robot with 10 links.

In order to get a machine-independent metric of how efficient our control law is, we used the `FLOPS()` function [37] to compute the number of floating-point operations each time our control law is computed. For a snake robot with 4 links, the number of required flops is 7956. For a snake robot with 10 links, the number of required flops is 91614. By considering a conservative value of 10 million flops per second as computational capability for the snake robot's controller, the time needed for the algorithm computation would be less than 1 ms for a snake robot with 4 links and less than 10 ms for a snake robot with 10 links. $\triangle$

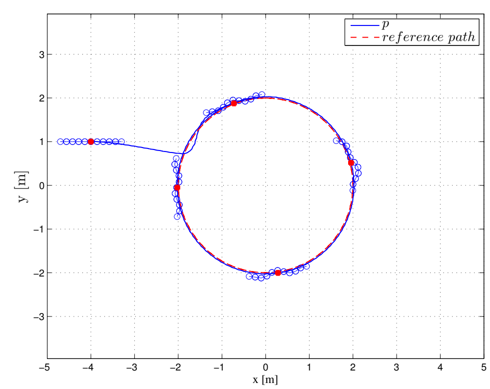

Fig. 3. Plots of the snake robot with 10 links and the path of its center of mass. An animation can be found at https://www.youtube.com/watch?v=Bkgi9AdcbSo.

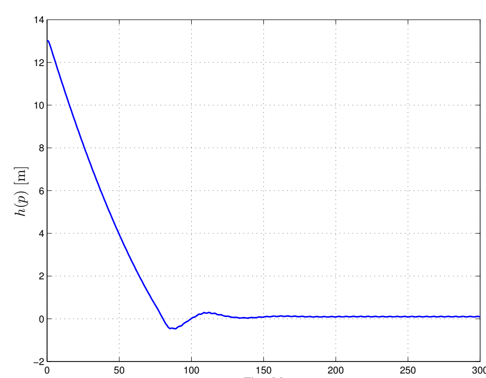

Fig. 4. The path following error.

Remark 9.3. **(Implementation of the Controller)** The camera-based position measurement system of the robot Wheeko enables us to calculate the global frame coordinates

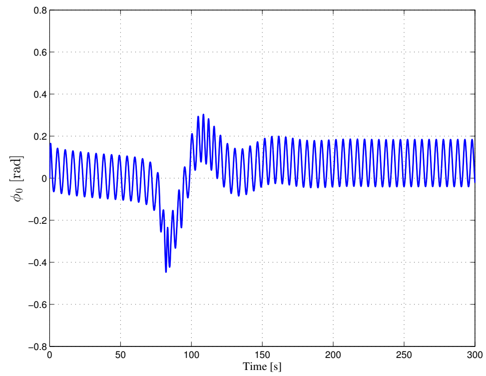

Fig. 5. The dynamic variable ϕ_0 remains uniformly ultimately bounded.

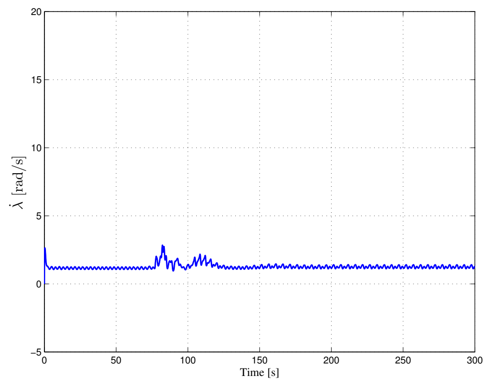

Fig. 6. The dynamic variable $\dot{\lambda}$ remains uniformly ultimately bounded.

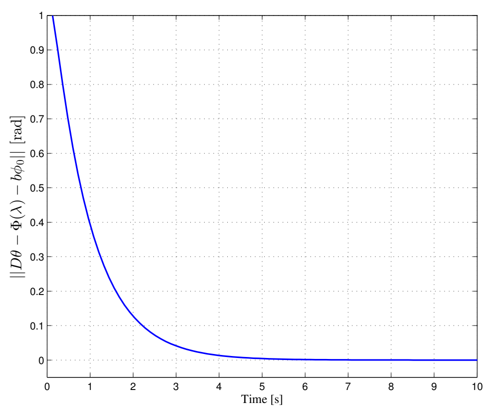

Fig. 7. The lateral undulatory gait (13) is stabilized among the shape variables of the snake robot.

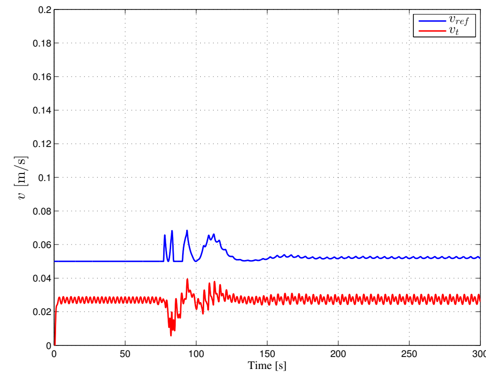

Fig. 8. Reference and actual tangential velocities.

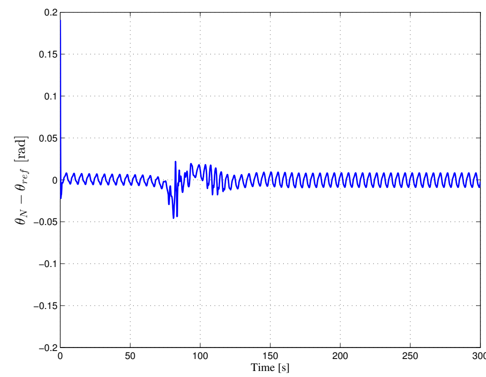

Fig. 9. The head angle tracking error.

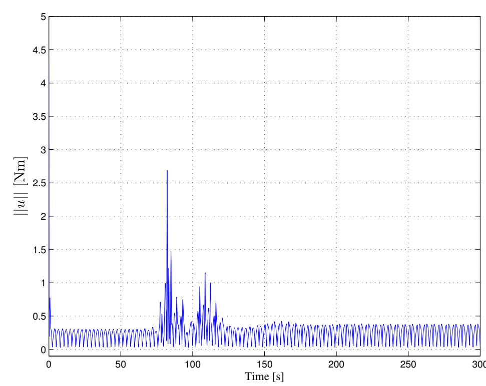

Fig. 10. Norm of the control torque vector.

of the head link, (x_N, y_N), and the absolute angle of the head link θ_N (see [10] for more details). Also, the snake robot's magnetic encoders measure the joint angles, i.e., the vector $\phi = [\phi_1, \ldots, \phi_{N-1}]^T$ is available from measurements, instead of the absolute link angles. We can use the following kinematic relationships to calculate the center of mass position, p, and the vector of absolute link angles, $\boldsymbol{\theta}$: $\boldsymbol{\theta} = H\phi + e\theta_N$, $p = \frac{-l}{N}\begin{bmatrix} e^T HA\cos(\boldsymbol{\theta}) \\ e^T HA\sin(\boldsymbol{\theta}) \end{bmatrix} + \begin{bmatrix} x_N \\ y_N \end{bmatrix}$. $\triangle$

Robustness analysis for circle tracking. We now test the robustness of the path following controller (57)–(61) to uncertainties in the friction parameters and to noise in the joint angle and center of mass measurements. Specifically, we present three tests.

Test 1. To simulate the inaccuracy of the encoder measurements, we replace θ in the feedback law (57)–(61) by $\theta + n(t)$, where $n(t)$ is a vector of zero average white Gaussian noise signals whose standard deviation σ is 10% of the maximum joint angle observed in steady-state under nominal operation, $\sigma = 0.1 \cdot \max_i \limsup_t |\theta_i(t) - \theta_{i+1}(t)|$. In our simulations we found $\sigma = 0.07$ rad, or approximately 4 degrees. This is quite high, as in practical experiments with the snake robot Wheeko the angle measurements are seen to be accurate within 1-2 degrees.

Test 2. Here we simulate errors in the measurement of the center of mass position, p. To this end, we replace p with $p + n(t)$ in the feedback law (57)–(61), where $n(t)$ is a vector of white Gaussian noise signals with standard deviation 0.1 m. While the camera tracking system in the NTNU Snake Robotics Laboratory has sub-millimeter accuracy, we have chosen this large measurement error to reflect that in the absence of an indoor camera system, position estimation would have to rely on on-board camera data and suitable vision algorithms. In this setting, it is reasonable to assume a measurement error of the order of 0.1 m.

Test 3. Since mass and moments of inertia can be determined with high accuracy, the most relevant parametric modelling uncertainty is in the friction coefficients c_n and c_t. In this test, we replace c_n and c_t by $0.9c_n$ and $0.9c_t$ in the feedback law (57)–(61). This corresponds to a 10% uncertainty in these parameters.

Performance metrics. In order to assess the robustness of the feedback law (57)–(61) in the three tests above, we use four performance metrics:

- The first performance metric, P_1, is the RMS value of the path following error $h(p(t)) = p_x^2(t) + p_y^2(t) - 4$ in steady-state.
- The second performance metric, P_2, is the settling time of the path following error: the largest time after which the absolute value of the path following error remains within one third of its initial value.
- The third performance metric, P_3, is the largest torque magnitude applied to each individual joint, i.e, $\sup_t(\max_i |u_i(t)|)$, $1 \leq i \leq N-1$. This value should remain within the physical actuator limit of 7 Nm.
- Finally, P_4 represents the RMS value of the torque norm signal $\|u(t)\|$ in steady-state.

The results of the tests are found in Table III. In order to examine the influence of the measurement noise on the performance of the controller in Tests 1 and 3, we ran the same tests for 10 times, and took the average of the results. In the table, Test 0 corresponds to the nominal situation where there are no noise and modelling uncertainty in the simulation. The results in the table illustrate the robustness of the proposed controller. Specifically, the performance of the controller is only marginally affected by noise in the angle measurements and uncertainty in the friction coefficients (Tests 1 and 3). Also, the peak torque remains within the physical actuator limit of 7 Nm. Furthermore, as it is shown in Remark 5.1, the peak and the RMS torques decrease slightly with decreasing friction coefficients in Test 3. In Test 2, the large noise in the center of mass position measurement has no significant effect on the settling time, and it causes a gracious degradation of the RMS value of the path following error, which increases from 0.1 m to approximately 0.2 m. However, we note that the peak torque in this case exceeds the actuator limit. The degraded performance in Test 2 is not surprising, since the position measurement error is in the magnitude of the snake robot's link length in this test.

As we mentioned in the Introduction, the intrinsic robustness of the VHC controller is to be ascribed to the fact that this controller does not rely on any exogenous reference signal. This general principle can be roughly explained as follows. A feedback control loop aimed at tracking a reference signal reacts to errors between the system output and the reference. As such, it attempts to make the output conform to the timing of the reference signal. When the loop is affected by uncertainties or disturbances, it may happen that the time parametrization of the reference signal becomes unfeasible in that the system output cannot "keep up" with the reference. In such a situation, the loop will measure a large tracking error and the overall performance will be affected. On the other hand, if the time parametrization is removed from the loop and the control objective of tracking is replaced by the stabilization of a suitable relation (the VHC in this paper), then the control loop no longer mandates a specific time parametrization for the output. It only requires the enforcement of the implicit relation. Such a loop, therefore, is completely insensitive to issues of timing of the reference signal, and typically displays a greater robustness to uncertainties or disturbances. We will illustrate this principle next.

TABLE III
ROBUSTNESS ANALYSIS FOR CIRCLE TRACKING

Test No.	P_1	P_2	P_3	P_4
0	0.1 m	47.2895 sec	2.775 Nm	0.2887 Nm
1	0.1071 m	48.6097 sec	2.9136 Nm	1.9076 Nm
2	0.2056 m	47.4095 sec	11.8068 Nm	3.2157 Nm
3	0.1 m	47.2895 sec	2.6894 Nm	0.2708 Nm

Performance indicators for the VHC controller (57)–(61) in the presence of noise in the angle measurements (Test 1), noise in the center of mass position measurements (Test 2), and uncertainty in the friction coefficients (Test 3). Test 0 refers to the nominal performance of the robot in the absence of noise and uncertainties.

Comparison with PD control. We now compare the performance of the proposed VHC controller (57)–(61) with the PD controller proposed in [18]. Since the results in [18] are only applicable to straight line paths, the comparison is made based on straight line path following. In the VHC controller, this corresponds to setting $h(p) = [0 \;\; 1]p$. Accordingly, we let the path be the horizontal straight line $p_y = 0$. Let $\bar{\theta} = \frac{1}{N}\sum_{i=1}^{N} \theta_i$ denote the heading (or orientation) of the snake robot. The PD control law from [18] is given as follows:

$$u_i = k_p(\phi_{i,\mathrm{ref}} - \phi_i) - k_d\dot{\phi}_i, \tag{64}$$

where

$$\phi_{i,\mathrm{ref}} = \alpha \sin(\omega t + (i-1)\delta) + \phi_0. \tag{65}$$

The joint angle offset is determined according to the following law:

$$\phi_0 = k_\theta(\bar{\theta} - \bar{\theta}_{\mathrm{ref}}), \tag{66}$$

where $\bar{\theta}$ is the mean of the link angles and

$$\bar{\theta}_{\mathrm{ref}} = -\arctan(\frac{p_y}{\Delta}), \tag{67}$$

where $\Delta > 0$ is a design parameter referred to as the look-ahead distance.

The gains of the VHC controller (57)–(61) are once again found in Table II. The gains of the PD controller are chosen to be $k_p = 10$, $k_d = 0.25$, $k_\theta = -1$ and $\Delta = 2$. Also, we set $\alpha = 40\pi/180$ rad, $\omega = 70\pi/180$ rad/sec, and $\delta = 75\pi/180$ rad. This choice is made in such a way that, when using the PD controller in the absence of noise and modelling uncertainty, the RMS value of the path following error in steady-state is equal to that of the VHC-based controller. Moreover, the settling times of the path following error of the two controllers are approximately the same.

In Table IV we present a comparison of the four performance metrics P_1–P_4 for the two controllers in response to the four tests 0–3 defined in the previous section. Similar to the circle tracking simulations, we ran Tests 1 and 3 for 10 times, and took the average of the results. While in all tests, the settling times of the two controllers are comparable, we see from the table that in Tests 1 and 2 (robustness to angle and position noise), the value of the RMS path following error of the PD controller (indicator P_1) is 40% worse than that of the VHC controller. In Test 3 (uncertainty in friction coefficients) indicator P_1 is the same for the two controllers. Finally, in all tests the RMS value of the torque norm of the PD controller (indicator P_4) is larger that of the VHC controller, and in Test 2, the peak torque (indicator P_3) of the PD controller exceeds the physical limit of 7 Nm. In conclusion, the VHC controller proposed in this paper outperforms the PD controller of [18], while requiring significantly less control effort. This observation confirms the rationale presented earlier about the intrinsic robustness of controllers not relying on exogenous reference signals. In particular we posit that the larger control effort required by the PD controller is due to the fact that measurement noise and friction uncertainties cause the tracking error to be artificially large.

TABLE IV
ROBUSTNESS ANALYSIS OF VHC AND PD CONTROLLERS FOR STRAIGHT LINE PATH FOLLOWING

Test	P_1	P_2	P_3	P_4
VHC–0	0.0015 m	58.3691 sec	0.5962 Nm	0.2345 Nm
PD–0	0.0015 m	58.3691 sec	2.7307 Nm	0.2717 Nm
VHC–1	0.0054 m	60.0858 sec	3.4265 Nm	1.8731 Nm
PD–1	0.0143 m	63.5193 sec	3.9407 Nm	1.9034 Nm
VHC–2	0.0095 m	58.3702 sec	4.2266 Nm	0.3764 Nm
PD–2	0.0161 m	64.8069 sec	12.1186 Nm	1.6271 Nm
VHC–3	0.0015 m	58.4022 sec	1.2062 Nm	0.2345 Nm
PD–3	0.0015 m	58.3691 sec	2.7307 Nm	0.2717 Nm

Comparison of the performance of the VHC controller (57)–(61) and the PD controller of [18] in the case of straight line path following.

X. DISCUSSION

The simulation results presented in this section validate the performance of the proposed control strategy. The given approach is to our best knowledge the first analytically designed maneuvering controller for snake robots without nonholonomic constraints, which presents formal stability proofs for the controlled system. Among the advantages of this approach is that it is analytical in the sense that the effect of changes in any given control or robot parameter on the controlled system can be investigated through the mathematical analysis given throughout the paper. Consequently, through formal stability analysis we can guarantee the convergence of the state variables to their references. Furthermore, since the stability proofs were derived for general N, J, and m, then the approach can be used for any robotic snake with any inertial parameters. We have also validated the performance of the controller in the presence of reasonably large measurement noise in the simulations. A main topic of future work is to implement the controllers on a robotic snake to validate the practical effectiveness of the approach. As it can be seen from the simulations, the performance of the VHC controller is good and according to what is predicted by Theorem 8.1. Our control design shows some degree of robustness to modelling errors and noise. In particular, our controller shows a more robust performance in response to modelling errors and noise in comparison with the PD controller. In terms of implementation of the controller one might saturate the output of the two dynamic compensators and use anti-windup design. A main advantage of the proposed maneuvering controller is that it can be applied to any type of existing wheel-less snake robots. In particular, provided that the electric motors mounted on the joints of a typical snake robot can provide enough torque, the proposed control laws can be used for any snake robot with any given mass, moments of inertia, number of links, while moving on a planar surface with any friction properties. For practical implementations, actuator saturations will present limitations on the achievable torques and torque rates, and the tuning must be done accordingly. The gain tuning will thus be a trade-off between making the ultimate bound on ϕ_0 from Proposition 6.1 sufficiently small and staying within the actuator limitations.

XI. CONCLUSIONS

We considered the problem of path following control for a planar snake robot. We defined $N-1$ constraint functions for directly actuated shape variables of the robot. These constraint functions were dependent on the variations of the states of dynamic compensators which were used to control the head angle and the forward velocity of the robot on the constraint manifold. The given approach is to our best knowledge the first analytically designed maneuvering controller for snake robots without nonholonomic constraints, which presents formal stability proofs for the controlled system. Simulation results were presented that illustrate and validate the theoretical results. In future work, an experimental validation and also an extension of our solutions to non-smooth paths will be pursued.

REFERENCES

[1] S. Hirose, *Biologically Inspired Robots: Snake-Like Locomotors and Manipulators*. Oxford University Press, 1993.

[2] C. Ye, S. Ma, B. Li, and Y. Wang, "Turning and side motion of snake-like robot," in *IEEE Int. Conf. Robot. Autom.*, vol. 5, 2004, pp. 5075–5080.

[3] M. Sato, M. Fukaya, and T. Iwasaki, "Serpentine locomotion with robotic snakes," *IEEE Control Systems Magazine*, vol. 22, no. 1, pp. 64–81, 2002.

[4] F. Matsuno and H. Sato, "Trajectory tracking control of snake robots based on dynamic model," in *Proc. IEEE Int. Conf. Robot. Autom.*, 2005, pp. 3029–3034.

[5] Y. Hoshi, M. Sampei *et al.*, "Locomotion control of a snake-like robot based on dynamic manipulability," in *Proc. IEEE/RSJ Int. Conf. Intell. Robot. Syst.*, vol. 3, 2000, pp. 2236–2241.

[6] M. Tanaka and F. Matsuno, "Control of 3-dimensional snake robots by using redundancy," in *Proc. IEEE Int. Conf. Robot. Autom.*, 2008, pp. 1156–1161.

[7] S. Ma, Y. Ohmameuda, K. Inoue, and B. Li, "Control of a 3-dimensional snake-like robot," in *Proc. IEEE Int. Conf. Robot. Autom.*, 2003, pp. 2067–2072.

[8] M. Tanaka and F. Matsuno, "A study on sinus-lifting motion of a snake robot with switching constraints," in *Proc. IEEE Int. Conf. Robot. Autom.*, 2009, pp. 2270–2275.

[9] P. Prautsch, T. Mita, and T. Iwasaki, "Analysis and control of a gait of snake robot," *TRANSACTIONS-INSTITUTE OF ELECTRICAL ENGINEERS OF JAPAN D*, vol. 120, no. 3, pp. 372–381, 2000.

[10] P. Liljebäck, K. Y. Pettersen, Ø. Stavdahl, and J. T. Gravdahl, *Snake Robots: Modelling, Mechatronics, and Control*. Springer, 2013.

[11] K. A. McIsaac and J. P. Ostrowski, "Motion planning for anguilliform locomotion," *IEEE Trans. Robot. Autom.*, vol. 19, no. 4, pp. 637–652, 2003.

[12] G. Hicks and K. Ito, "A method for determination of optimal gaits with application to a snake-like serial-link structure," *IEEE Trans. Automat. Contr.*, vol. 50, no. 9, pp. 1291–1306, 2005.

[13] S. Ma, Y. Ohmameuda, and K. Inoue, "Dynamic analysis of 3-dimensional snake robots," in *Proc. IEEE/RSJ Int. Conf. Intell. Robot. Syst.*, vol. 1, 2004, pp. 767–772.

[14] S. Toyoshima, M. Tanaka, and F. Matsuno, "A study on sinus-lifting motion of a snake robot with sequential optimization of a hybrid system," *IEEE Trans. Autom. Sci. Eng.*, vol. 11, no. 1, pp. 139–144, 2014.

[15] R. L. Hatton, R. A. Knepper, H. Choset, D. Rollinson, C. Gong, and E. Galceran, "Snakes on a plan: Toward combining planning and control," in *Proc. IEEE Int. Conf. Robot. Autom.*, 2013, pp. 5174–5181.

[16] E. A. Cappo, M. Travers, and H. Choset, "Head-orientation for a sidewinding snake robot using modal decomposition," in *Proc. SPIE 9084, Unmanned Systems Technology XVI, 90840K*, 2014.

[17] S. Ma, "Analysis of creeping locomotion of a snake-like robot," *Advanced Robotics*, vol. 15, no. 2, pp. 205–224, 2001.

[18] P. Liljebäck, K. Y. Pettersen, Ø. Stavdahl, and J. T. Gravdahl, "Controllability and stability analysis of planar snake robot locomotion," *IEEE Trans. Automat. Contr.*, vol. 56, no. 6, pp. 1365–1380, 2011.

[19] P. Liljebäck, I. U. Haugstuen, and K. Y. Pettersen, "Path following control of planar snake robots using a cascaded approach," *IEEE Trans. Control Syst. Tech.*, vol. 20, no. 1, pp. 111–126, 2012.

[20] E. Rezapour, K. Y. Pettersen, P. Liljebäck, and J. T. Gravdahl, "Path following control of planar snake robots using virtual holonomic constraints," in *Proc. IEEE Int. Conf. Robot. Biomim.*, 2013, pp. 530–537.

[21] E. Rezapour, K. Y. Pettersen, P. Liljebäck, J. T. Gravdahl, and E. Kelasidi, "Path following control of planar snake robots using virtual holonomic constraints: theory and experiments," *Robotics and Biomimetics, SpringerOpen*, 2014.

[22] A. Mohammadi, E. Rezapour, M. Maggiore, and K. Y. Pettersen, "Direction following control of planar snake robots using virtual holonomic constraints," in *53rd IEEE Conf. on Decision and Control*, Los Angeles, CA, 2014.

[23] E. Rezapour, A. Hofmann, K. Pettersen, A. Mohammadi, and M. Maggiore, "Virtual holonomic constraints based direction following control of planar snake robots described by a simplified model," in *IEEE Multi-Conf. on Systems and Control*, Antibes, France, 2014.

[24] E. Rezapour, A. Hofmann, and K. Y. Pettersen, "Maneuvering control of planar snake robots described by a simplified model," in *IEEE Int. Conf. on Robot. Biomim.*, Bali, Indonesia, 2014.

[25] P. Liljebäck, K. Y. Pettersen, Ø. Stavdahl, and J. T. Gravdahl, "A review on modelling, implementation, and control of snake robots," *Robotics and Autonomous Systems*, vol. 60, no. 1, pp. 29–40, 2012.

[26] J. Nakanishi, T. Fukuda, and D. E. Koditschek, "A brachiating robot controller," *IEEE Trans. Robotic Autom.*, vol. 16, no. 2, pp. 109–123, 2000.

[27] F. Plestan, J. W. Grizzle, E. R. Westervelt, and G. Abba, "Stable walking of a 7-DOF biped robot," *IEEE Trans. Robotic Autom.*, vol. 19, no. 4, pp. 653–668, 2003.

[28] A. Shiriaev, J. W. Perram, and C. Canudas-de Wit, "Constructive tool for orbital stabilization of underactuated nonlinear systems: Virtual constraints approach," *IEEE Trans. Automat. Contr.*, vol. 50, no. 8, pp. 1164–1176, 2005.

[29] M. Maggiore and L. Consolini, "Virtual holonomic constraints for Euler-Lagrange systems," *IEEE Trans. Automat. Contr.*, vol. 58, no. 4, pp. 1001–1008, 2013.

[30] P. Seibert and J. S. Florio, "On the reduction to a subspace of stability properties of systems in metric spaces," *Annali di Matematica pura ed applicata*, vol. CLXIX, pp. 291–320, 1995.

[31] M. El-Hawwary and M. Maggiore, "Reduction theorems for stability of closed sets with application to backstepping control design," *Automatica*, vol. 49, no. 1, pp. 214–222, 2013.

[32] G. La Spina, M. Sfakiotakis, D. P. Tsakiris, A. Menciassi, and P. Dario, "Polychaete-like undulatory robotic locomotion in unstructured substrates," *IEEE Trans. Robot.*, vol. 23, no. 6, pp. 1200–1212, 2007.

[33] H. K. Khalil, *Nonlinear Systems*. Prentice Hall, 3rd edn., 2002.

[34] A. Isidori, *Nonlinear control systems II*. Springer, London, 1999.

[35] M. Nagumo, "Über die lage der integralkurven gewöhnlicher differentialgleichungen," *Proc. Phys.-Math. Soc. Japan (3)*, vol. 24, pp. 551–559, 1942.

[36] F. Morabito, A. R. Teel, and L. Zaccarian, "Results on anti-windup design for Euler-Lagrange systems," in *Proc. IEEE Int. Conf. Robot. Autom.*, 2002, pp. 3442–3447.

[37] Qian, Hang (2015). Counting the Floating Point Operations (FLOPS), MATLAB Central File Exchange, No. 50608, Ver. 1.0, Retrieved June 30, 2015.

Alireza Mohammadi received the M.Sc. degree in electrical and computer engineering from the University of Alberta, Edmonton, Canada, in 2011. He is currently pursuing the Ph.D. degree in the Department of Electrical and Computer Engineering at the University of Toronto, Ontario, Canada. His research interests include nonlinear control theory, robotics and motion control of underactuated mechanical systems.

Ehsan Rezapour received the M.Sc. degree in robotics and control from the Department of Applied Physics and Electronics, UmeåUniversity, Umeå, Sweden, in 2011, and the Ph.D. degree in Automatic Control from the Department of Engineering Cybernetics, Norwegian University of Science and Technology (NTNU), Trondheim, Norway, in 2015.

During the autumn semester in 2013 he was a visiting graduate student at the Department of Electrical and Computer Engineering, University of Toronto, Ontario, Canada. He is currently an Automation and Process Control Engineer at Norsk Titanium AS in Honefoss, Norway, working on developing closed-loop control methods for metal-based additive manufacturing process. His research interests include motion control of underactuated mechanical systems, locomotion control of biologically-inspired robots, nonlinear and geometric control, and multivariable process control with applications to additive manufacturing.

Manfredi Maggiore was born in Genoa, Italy. He received the "Laurea" degree in electronic engineering in 1996 from the University of Genoa and the Ph.D. degree in electrical engineering from Ohio State University, USA, in 2000. Since 2000 he has been with the Edward S. Rogers Sr. Department of Electrical and Computer Engineering, University of Toronto, Canada, where he is currently Professor. He has also been a visiting Professor at the University of Bologna (2007–2008). His research focuses on mathematical nonlinear control, and relies on methods from dynamical systems theory and differential geometry.

Kristin Y. Pettersen is a Professor in the Department of Engineering Cybernetics, Norwegian University of Science and Technology (NTNU). She was Head of Department 2011-2013 and Director of the NTNU ICT Programme of Robotics 2010-2013. In 20132022 she is Key Scientist at the CoE AMOS. She received the MSc and PhD degrees in Engineering Cybernetics at NTH/NTNU in 1992 and 1996. She has published 200 papers for conferences and journals, and her research interests focus on nonlinear control of mechanical systems, with a special emphasis on marine robotics and snake robotics. She has co-edited the Springer Verlag book "Group Coordination and Cooperative control", and is co-author of "Snake Robots" and "Modeling and Control of Vehicle-Manipulator Systems". She is an Associate Editor of IEEE Transactions on Control Systems Technology and IEEE Control Systems Magazine. She was a member of the Board of Governors of IEEE Control Systems Society 2012-2014.